Invited paper

Surface waves in deep and shallow waters

OCEANOLOGIA, 52 (1), 2010.
pp. 5–52.

KEYWORDS
Surface waves
Non-linear interactions
Energy dissipation
Aerosol fluxes

Stanisław R. Massel

Institute of Oceanology
of the Polish Academy of Sciences,
Powstańców Warszawy 55, PL–81–712 Sopot, Poland

Received 8 January 2010, revised 24 February 2010, accepted 10 March 2010.

Abstract

The motion of water due to surface waves is the most dynamic factor observed in the marine environment. In this review various aspects of the wave modelling of non-linear, steep surface waves and their role in the atmosphere-ocean interaction are discussed. Significant improvements in wave forecasting have been made in the last ten years. This is to a large extent related to substantial progress in the description of wind forcing and other processes, as well as to the more efficient use of satellite observations and assimilation methods. One striking observation is the increasing variety and complexity of models in which more physical processes are implemented, greater precision and resolution achieved and extended ranges of applicability demonstrated. However, in order to evaluate the applicability of particular models, comparison with high quality experimental data, collected in nature or under laboratory conditions, is necessary.

Notation list

a – wave amplitude, constant
a_1 – function

ak	–	wave steepness
$a_z^{(E)}$	–	Eulerian downward acceleration
$a_z^{(L)}$	–	Lagrangian downward acceleration
a_γ	–	coefficient
A	–	complex amplitude, constant
A_{br}	–	critical amplitude
A_{rms}	–	root-mean-square amplitude
$\tilde{A}$	–	non-dimensional complex amplitude
b	–	constant
C	–	phase velocity
C_{br}	–	phase speed of breaking waves
C_{fr}	–	bottom friction coefficient
C_g	–	group velocity
C_+, C_-, φ	–	functions of interaction coefficients
C_θ	–	phase velocity in θ – space
C_σ	–	phase velocity in σ – space
D_b	–	dissipation factor due to wave breaking
D_{fr}	–	energy-dissipation rate due to bottom friction
$D(\theta)$	–	directional spreading function
$E_{dissrate}$	–	rate of energy loss
E_{diss}	–	energy dissipation for a very narrow spectrum
f	–	probability density function
F_{br}	–	probability of wave breaking
F_{cov}	–	percentage of sea surface covered by breaking waves
$F(\mathbf{k})$	–	wave number spectrum
h	–	water depth
H_s	–	significant wave height
$H_{\max}$	–	max. wave height
I_c, I_s	–	integrals
I_0	–	modified Bessel function
$I(s)$	–	spreading function
J_0,J_1	–	Bessel functions of the first kind
k_c	–	carrier wave number
$\mathbf{k}$	–	wave number vector
K_T	–	transmission coefficient
m_n	–	spectral moment of the nth-order
N	–	wave action density
N_b	–	number of breaking waves per wave

$R_{\max}$	–	max. run-up height
s	–	directional spreading parameter
S	–	source function
S_{diss}	–	source term due to energy loss
s	–	directional spreading parameter
S	–	source function
S_{diss}	–	source term due to energy loss
S_{in}	–	source term due to input from wind
S_{nl}	–	source term due to non-linear interaction
$S(\omega, \theta)$	–	two-dimensional frequency spectrum
T	–	wave period
u_*	–	friction velocity
$u_{rms,bottom}$	–	root-mean-square orbital velocity at bottom
V_{10}	–	wind speed at 10 m altitude
w	–	vertical velocity component
X	–	wind fetch
Z_0	–	function of propagation mode
Z_n	–	function of evanescent mode
Z_{-1}	–	function of sloping mode
α	–	constant
β	–	Phillips' constant
β_1	–	bottom slope
β_K	–	growth rate due to Krasitskii
β_x, β_{BF}	–	growth rate by Benjamin & Feir
γ	–	peak enhancement factor
γ_{br}	–	energy dissipation due to wave breaking
γ_{fr}	–	energy dissipation due to bottom friction
γ_1	–	numerical constant
δ	–	small non-dimensional quantity
Δ	–	relative local energy growth rate
ϵ	–	small quantity
ε_d	–	dominant wave steepness
ε_l	–	local surface slope
ε_s	–	significant steepness
ε_{th}	–	threshold steepness

ζ – surface wave ordinate
$\zeta_{\max}$ – max. crest height

$\overline{\eta}$ – mean water level

θ – wave component direction, inclination of a breaking wave's forward face

ρ_a – density of air
ρ_w – density of water

σ – intrinsic frequency

ω_c – carrier wave frequency
ω_p – peak frequency of wave spectra
Ω, ω – observed (absolute) frequency

1. Introduction

The atmosphere and ocean form a coupled system which continuously exchanges heat, momentum and mass at the air-sea interface. Owing to energy flow from the atmosphere to the ocean, this interface presents an aerodynamically rough surface that can consist of dynamic, unsteady, very high and steep surface waves. The hydrodynamics of this process is still not fully understood.

In the past, the study of surface wave mechanics concentrated predominantly on two aspects. On the one hand, wave mechanics was treated as a purely mathematical problem, important in numerical modelling (Lamb 1932, Stoker 1957, Phillips 1977, Le Blond & Mysak 1978, Davidan et al. 1978, 1985, Mei 1989, Komen et al. 1994, Massel 1989, 1996, Ochi 1998, Lavrenov 2003, Holthuijsen 2007). On the other, flow kinematics due to surface waves was used to estimate the resultant loadings on offshore and coastal structures under extreme and operating conditions. Textbooks and scientific papers provide many examples of the direct applications of wave mechanics to ocean and coastal engineering (Krylov et al. 1976, 1986, Sarpkaya & Isaacson 1981, Dean & Dalrymple 1998, Goda 2000, Mei et al. 2006).

However, in recent years, the focus has been redirected to climate change and the role played by the oceans. The interaction between the ocean and atmosphere at the air-sea interface is critical to our understanding of the Earth's climate as the ocean surface forms a filter to the exchange of heat, moisture, momentum and trace constituents (Massel 2007). In particular, the energy transfer from the atmosphere to the ocean enhances the heat flux and mixed layer during the circulation of the upper ocean, while the

energy fluxes from the ocean to the atmosphere affect gas and aerosol concentrations, as well as the atmospheric circulation, weather and climate.

This review examines the physics and modelling of non-linear, steep surface waves and their role in the atmosphere-ocean interaction. A detailed description of particular wave models is not given here, but the governing equations and references to the subject literature are used to illustrate the structure of particular models.

For the presentation of the problems it is useful to distinguish between deep ocean and shallow waters. In both cases, the dominant physical wave processes are characterised first. To a large extent these processes determine the selection of suitable mathematical and numerical models. Moreover, special wave events, such as whitecapping, freak waves, tsunamis and wave-induced groundwater circulation, are discussed. Knowledge of these events is of special importance for modern oceanography, and oceanic and coastal technology.

For the purposes of this paper, Table 1 classifies in a simple way the various types of waves and sets out suggested methods for their solution. Although such a classification is not unique, it will provide some useful insight into the complexity of surface waves.

The paper is organised as follows. The energy balance equation for deep water waves and its constituents are discussed in Section 2: particular

Table 1. Classification of surface waves and possible methods for their solution

Type of waves	Methods of solution
linear sinusoidal wave (typical of deep seas)	small amplitude wave theory for $H/h \ll 1$, $L/h < 10$ and $Ur = \left(\frac{H}{h}\right)\left(\frac{L}{h}\right)^2 < 75$
Stokes short waves (typical of intermediate wave depths)	5th order approximation (see Fenton 1985) for $H/h \leq 1$, $L/h < 10(20)$ and $Ur > 75$
long, cnoidal and solitary waves (typical of shallow water)	a Boussinesq-type approximation (see Fenton 1986) or higher order cnoidal wave theory (see Fenton 1979) for $H/h \leq 1$, $L/h > 20(20)$ and $Ur > 75$
freak waves	simulation using a Schrödinger-type equation when $H_{\max}/H_s > 2$ at any depth
steep, near breaking waves	local solution by Sobey (1992) or Baldock & Swan (1994) and the fully non-linear model by Clamond & Grue (2001a, b)
tsunami waves	numerical solution on the global scale (see Kowalik et al. 2005); in the coastal zone-run-up, wave models with breaking (see Pelinovsky 1996)

emphasis is placed on the kinematics and dynamics of extreme waves as well as the link between sea surface state and aerosol fluxes. Section 3 deals with the motion of waves in shallow waters, including the interaction of waves with a porous seabed. Finally, Section 4 gives the main conclusions.

2. Waves in deep waters

2.1. Energy balance equation

Surface waves are mostly generated by winds. They are highly dispersive and interact with each other; however, the time of interaction is finite because each wave propagates with a different phase speed. Therefore, in practice, there is no need for detailed information regarding the phases of ocean waves. Knowledge about the distribution of wave energy over the wave number space $\mathbf{k}$ (e.g. wave number spectrum $F(\mathbf{k},t)$) or over the wave frequency ω and direction θ (e.g. the wave frequency-directional spectrum, $S(\omega,\theta,t)$) is normally sufficient. In order to derive the governing equations for functions $F(\mathbf{k},t)$ or $S(\omega,\theta,t)$, two methods are usually applied: the Hamiltonian approach (Zakharov 1968) or the Lagrangian approach (Luke 1967). The resulting action balance equation takes the form (Janssen 2004)

$$\frac{\partial N}{\partial t} + \nabla_{\mathbf{x}} \cdot (\nabla_{\mathbf{x}} \Omega N) - \nabla_{\mathbf{k}} \cdot (\nabla_{\mathbf{x}} \Omega N) = S = S_{in} + S_{nl} + S_{diss}, \tag{1}$$

in which the wave action density N is given by

$$N_{\mathbf{k}} = \frac{gF(\mathbf{k})}{\sigma} \tag{2}$$

and σ is the so-called intrinsic frequency:

$$\sigma = \sqrt{gk \tanh(kh)}, \tag{3}$$

where k is the wave number modulus $k = |\mathbf{k}|$ and h is the water depth.

The observed or absolute frequency Ω obeys the following dispersion relation:

$$\Omega = \mathbf{k} \cdot \mathbf{U} + \sigma, \tag{4}$$

in which $\mathbf{U}$ is the water current vector. The right-hand side of the equation describes the source function S, including the spectral input from wind (S_{in}), the net spectral flux of energy action through the wave number $\mathbf{k}$ by non-linear wave-wave interactions (S_{nl}) and the energy loss by wave breaking (S_{diss}).

Equation (1) gives us the rate of change in time of the action density spectrum due to advection with group velocity $\mathbf{C}_g = \nabla_{\mathbf{k}}\Omega$, to refraction

resulting from the temporal and spatial dependence of the local wavenumber, and due to physical processes contained in the source term S. Therefore the direction of wave energy transport is generally not normal to the wave crest when an ambient current is present. Moreover, the wave energy is not conserved as the wave propagates through a current. The conserved quantity is the wave action N defined in eq. (1) – see Bretherton & Garrett (1969). This equation is currently regarded as the starting point of many modern wave forecasting models (Massel 1996, Holthuijsen 2007).

Observations of the two-dimensional spectrum $F(\mathbf{k})$ are rare. It is much easier to obtain the frequency-directional spectrum based on the analysis of a time series at a given location. The relationship between both spectra takes the form:

$$S(\omega,\theta)d\omega d\theta = F(\mathbf{k})d\mathbf{k} = F(k,\theta)kdkd\theta; \tag{5}$$

thus:

$$S(\omega,\theta) = \frac{k}{C_g}F(k,\theta), \tag{6}$$

in which $C_g = \partial\omega/\partial k$ and θ is the direction of the particular wave component.

In the following we will discuss the processes included in the source term S in equation (1).

2.2. The generation of ocean waves by wind

This problem has led to much debate and much controversy. First of all, we are dealing with the extremely difficult problem of turbulent airflow over a surface varying in space and time. On the other hand, in order to measure the growth rate of waves by wind we have to make certain assumptions regarding the process that causes waves to grow as a result of the work done by the wind pressure on the sea surface. However, because of the small air-water density ratio, growth rates are small and a very accurate determination of amplitude and phase of the wave-induced pressure fluctuations is required.

Nevertheless, considerable progress in the prediction of wave growth has been made over the past 40 years. Substantial contributions were made in the mid-1950 s, when Phillips (1957) and Miles (1957) published their theories of wave generation by wind. Both theories are based on the assumption that wave growth is due to a resonance phenomenon. Phillips considered the resonant forcing of waves by turbulent pressure fluctuations, while Miles assumed resonant interaction between wave-induced pressure fluctuations and free surface waves. A consequence of this assumption is that Phillips' mechanism gives rise to a linear growth of the wave spectrum

in time, although this growth is independent of the spectrum itself. In the case of Miles' mechanism, wave growth is exponentially proportional to the spectrum.

Field measurements have shown an order of magnitude agreement with Miles' theory, although this still predicts energy-transfer rates that are smaller than measured values. One of the reasons for these discrepancies is that Miles' theory assumes inviscid airflow and so neglects the role of air turbulence. Moreover, non-linear effects such as wave-mean flow interaction have been neglected.

There have been several attempts to overcome these shortcomings by numerical modelling of the turbulent boundary layer flow over a moving water surface (Janssen 2004). Results from this modelling that include the effects of small-scale turbulence and effects of gustiness agree with Miles' theory for the case when the phase speed is smaller than the wind speed (young waves). However, when the phase speed is larger than the wind speed (old waves), numerical models predict wave damping in contrast to Miles' theory. These simulations clearly demonstrated that the generation of ocean waves is in fact an example of two-way interaction: as soon as the waves become sufficiently steep the associated wave-induced stress slows down the airflow. This should result in dependence of the air-sea momentum transfer on the sea state.

2.3. Non-linear wave-wave interaction

Ocean waves are usually regarded as weakly non-linear, dispersive waves, and the effect of non-linearity on wave propagation is the result of a perturbation expansion starting with linear, freely propagating waves. Theoretical and experimental studies provide convincing evidence that regular wave trains in deep water are liable to a number of instabilities that lead to wave breaking without external forcing. In particular, a small disturbance in the form of two modes with 'sideband' frequencies, adjacent to the fundamental frequency, will be forced to increase exponentially owing to non-linear interaction mechanisms, and primary wave motion becomes unstable due to this form of disturbance. Such instability of periodic wave trains is known as Benjamin-Feir instability. Benjamin & Feir (1967) examined a primary, deep-water wave of finite amplitude a and frequency ω superimposed by two 'sidebands' of infinitesimal amplitude ϵa and of frequencies $\omega(1 \pm \delta)$ respectively, where ϵ and δ are small quantities. They found that motion becomes unstable and the sidebands tend to grow in amplitude at the expense of the primary wave, provided that

$$2(ak)^2 > \delta^2. \tag{7}$$

Then the corresponding initial growth rate becomes

$$\beta_x = \frac{d(\ln a)}{d\,(kx)}, \tag{8}$$

which is presented by Benjamin & Feir (1967) in the form

$$\beta_x = \beta_{BF} = \varepsilon^2\,\hat{\delta}(2-\hat{\delta}^2)^{1/2}, \tag{9}$$

where $\varepsilon = ak$, $\hat{\delta} = \dfrac{\delta\omega}{\varepsilon\omega_c}$ and ω_c is the carrier frequency. The instability requires that $0 < \hat{\delta} \leq \sqrt{2}$, and the maximum growth appears when $\hat{\delta} = 1.0$.

However, the theory of Benjamin & Feir (1967) is asymptotically valid only for sufficiently small values of wave steepness ak and modulation frequency δ. In particular, Longuet-Higgins (1978) found that subharmonic instabilities of the Benjamin-Feir type are confined to waves whose 'steepness' ak lay within a certain finite range with the upper limit at $ak \approx 0.37$. The growth rate is about 14% per period, until $ak \approx 0.32$. As ak increases beyond ≈ 0.346, the wave modes become stable again. Comparison of the calculated growth rates showed good agreement with the observations reported by Benjamin (1967) in the wave steepness range $0.07 < ak < 0.17$.

The experimental and numerical study of Lake et al. (1977) showed that the evolution of a nonlinear wave train, in the absence of dissipative effects, exhibited the so-called 'Fermi-Pasta-Ulam' recurrence phenomenon, where the modulation periodically increases and decreases, and the wave form periodically returns to its previous form. Modulation was caused by the growth of the two dominant sidebands of the Benjamin-Feir instability at the expense of the carrier. For small steepness, the original near-three-wave system was almost recovered. Figure 1 gives an example of such a system. In Tulin & Waseda's (1999) wave tank experiment, a wave 1 m in length was considered whose initial wave carrier frequency $\omega_c = 1.23$ Hz, while the sideband frequencies were 1.12 Hz and 1.34 Hz. Indicated fetches in the wave tank were 3.6 m, 9.0 m, 14.4 m, 19.8 m, 25.2 m, 30.6 m, 36 m and 41.4 m. The maximum modulation was observed in the middle of the channel and the spectrum recovered at a fetch of 41.4 m.

When the initial steepness is large enough, wave trains experience strong modulations followed by demodulations with the spectral peak downshifted to a lower sideband. Recently, it was found that Krasitskii's modification of the Zakharov evolution equation (Zakharov 1968) for the four-wave interaction correctly predicts the major features of the energy increase in the lower sideband relative to the upper sideband (Krasitskii 1994, Tulin & Waseda 1999). Downshifting to a lower sideband of the spectral peak appears in the absence of breaking, which demonstrates the role of the balance between momentum losses and energy dissipation in the exchange

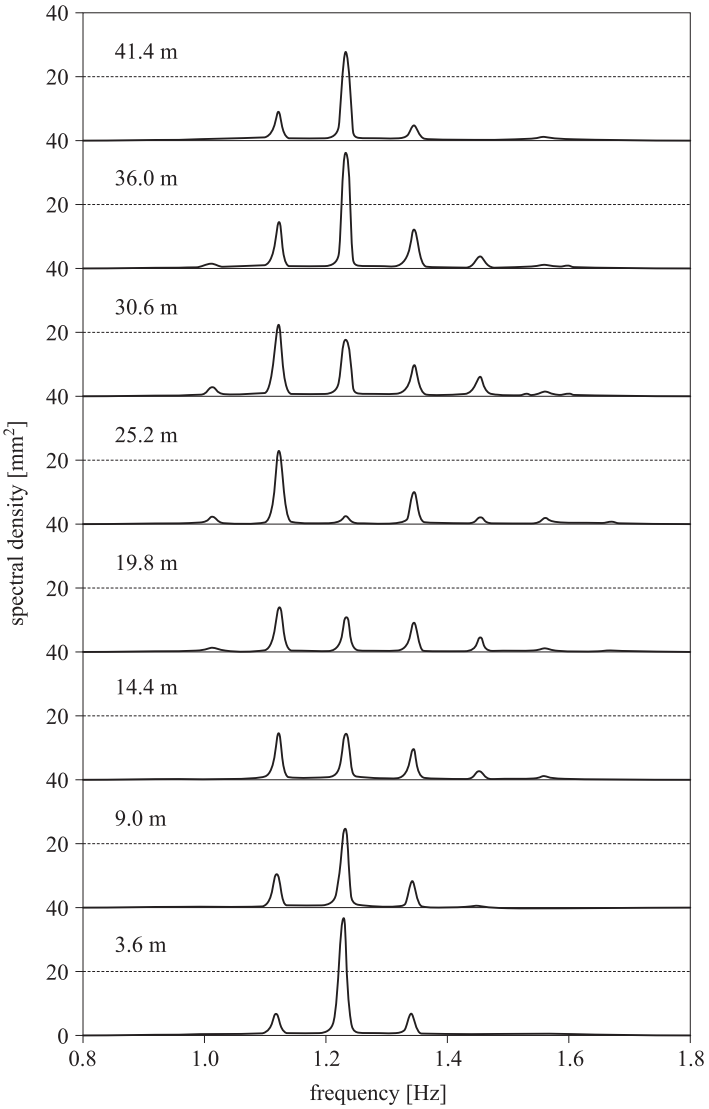

Figure 1. Fermi-Pasta-Ulam recurrence phenomenon (Tulin & Waseda 1999)

of energy between sidebands. Krasitskii's (1994) four-wave reduced equation yields the growth rate in the form

$$\beta_K = \varepsilon^2 \left(C_+ C_-\right)^{1/2} \sin\varphi, \tag{10}$$

in which C_+, C_- and φ are functions of interaction coefficients given in Krasitskii (1994). The experimental data of Waseda & Tulin (1999) have been compared with the theoretical predictions of Benjamin & Feir (1967) and Krasitskii (1994) (see Figure 2). Clearly, Benjamin and Feir's theory

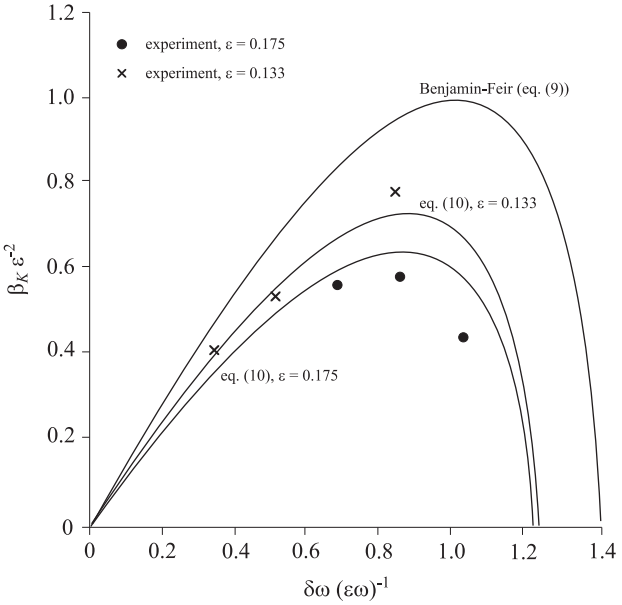

Figure 2. Comparison of the theoretical growth rate with experiments (Tulin & Waseda 1999)

overestimates the growth rate, but Krasitskii's solution agrees very well with measurements.

For a more complicated situation, analytical solutions of the evolution equations fail and only numerical simulations are possible. In particular, Dold & Peregrine (1986) established a connection between a weakly non-linear four-wave interaction process and a truly non-linear wave-breaking phenomenon (see also Song & Banner 2002, Banner & Song 2002). Dold & Peregrine showed that initial carrier wave steepness $(ak)_c$ differentiates between two modes of behaviour, i.e. recurrence of the initial state without breaking or the rapid onset of breaking. These two modes of behaviour are controlled by the non-dimensional relative local energy growth rate Δ:

$$\Delta = \frac{1}{\omega_c} \frac{D\overline{\chi^2}}{Dt}, \tag{11}$$

in which $\overline{\chi^2}$ is the mean relative local energy growth rate.

The recurrence happens when the maximum value of Δ is less than some threshold level Δ_{th}. Thus we have

$$\Delta_{\text{th}} = \begin{cases} < (1.30 - 1.50) \times 10^{-3} & - \quad \text{recurrence case} \\ > (1.30 - 1.50) \times 10^{-3} & - \quad \text{breaking case} \end{cases} \tag{12}$$

For wave breaking, the value of Δ continues to increase beyond the threshold level.

A common feature of the observed evolution is the fact that either for breaking or for recurrence towards the original wave group, the evolution induced by the non-linear group dynamics is accompanied by a systematic mean convergence of the energy density towards the local maximum of the evolving wave group.

The question now arises as to how the above discoveries may be used to predict wave propagation in practice. In particular, we are interested in a statistical description of the sea surface in terms of the evolution of the energy of an ensemble of waves when non-linear transfer gives rise to a downshift of the wave number. In order to conserve energy and wave action, considerable amounts of energy are transferred from the region just beyond the location of the spectral peak to the high wave number part of the spectrum. Therefore, the rate of change of the spectrum due to non-linear interactions demonstrates the typical three-lobe structure (Figure 3).

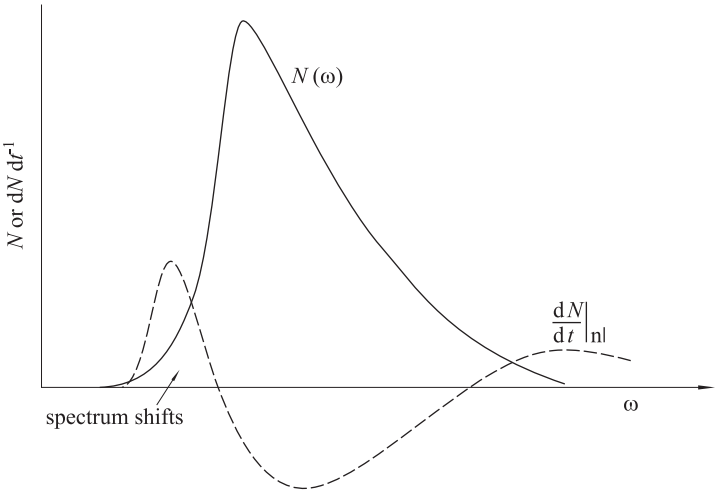

Figure 3. Three-lobe structure of the rate of change of the spectrum (Janssen 2004)

It should be noted that both resonant and non-resonant wave-wave interactions are included in the evolution equation. For short times the evolution of the wave action density N is due to both resonant and non-resonant quadruplet wave-wave interactions. However, the time scale on which non-resonant interactions operate is short, typically of the order of 10 to 20 wave periods. Thus, for wave prediction on the global scale there is interest only in the slow time evolution of the wave spectrum when only

resonant interactions contribute to spectral change. Numerical experiments using the exact non-linear transfer function suggest that the spectra tend to adjust in such a way that the directionally averaged spectra are close to $k^{-5/2}$ (or to $k^{-7/2}$ for the two-dimensional spectrum). This result follows from Kolmogorov's concept of an energy cascade when a constant non-linear energy flux is maintained through the system. Then the Kitaigorodskii (1983) scaling yields the frequency spectrum $S(\omega)$ in the form suggested by Toba (1973):

$$S(\omega) = 2A\left(\frac{\rho_a}{\rho_w}\right)^{1/2} u_* g \omega^{-4}, \tag{13}$$

where ρ_a and ρ_w are the air and water density respectively, u_* is the friction velocity, g is the acceleration due to gravity and A is a constant. The ω^{-4} law is typically valid for the frequency range (1.3–3.0)ω_p, where ω_p is the peak frequency of the waves.

Calculation of the S_{nl} term in eq. (1) requires an enormous computation effort. Thus, some form of parameterisation of S_{nl} is needed. After several past attempts there is now some consensus that the discrete interaction approximation (DIA) developed by Hasselmann et al. (1985) offers the best parameterisation of S_{nl}. It was incorporated into the well-known third-generation prediction model WAM4. For more information on the numerical implementation techniques for the energy balance equation, see, for example, WAMDI (1988), Janssen (2004) or Holthuijsen (2007).

2.4. Whitecap coverage and energy dissipation

2.4.1. Whitecap coverage of the sea surface

The energy flow from the atmosphere to the ocean generates an aerodynamically rough ocean surface. If the energy flow is sufficiently strong, at some points of the surface, waves lose their stability and eventually break in the form of whitecaps of various scales (see colour photo). The percentage of sea surface covered by whitecaps is usually parameterised in terms of the wind speed, when this speed is greater than about 4 m s^{-1}; below this speed, whitecaps are not observed. However, wind speed alone cannot fully parameterise the complex process of wave breaking and whitecap formation.

The rate of energy supplied by the wind is closely related to the wind stress and to the atmospheric stability conditions. Approximately, the percentage of sea surface covered by breaking waves F_{cov}, can be written in the form (Massel 2007)

$$F_{\mathrm{cov}} = a \cdot V_{10}^{b}, \tag{14}$$

where F_{cov} is expressed as percentage, V_{10} is the wind speed in m s^{-1} at 10 m altitude, while a and b are empirical constants. The experimental data (Monahan 1971, Stramska & Petelski 2003, Massel 2007) indicate that

$$10^{-7} < a < 10^{-5} \quad \text{and} \quad 3.0 < b < 3.75. \tag{15}$$

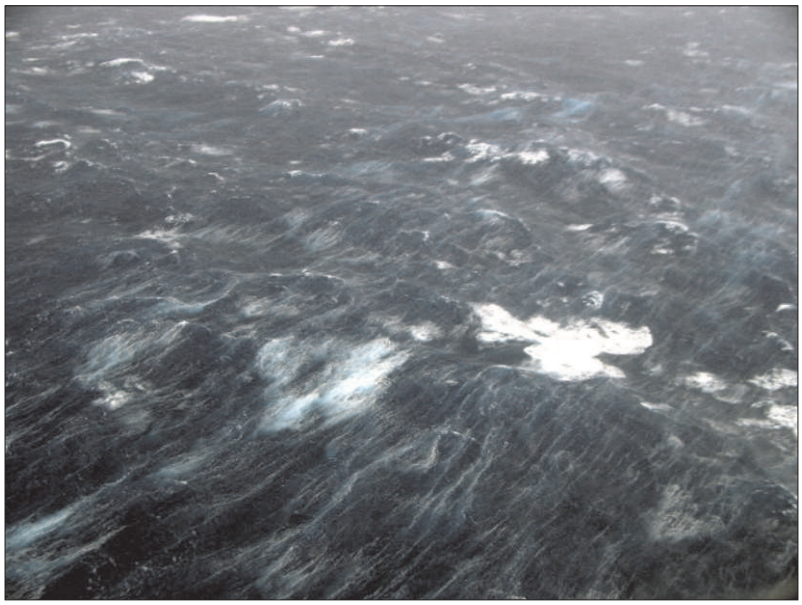

Photo 1. Whitecapping on the sea surface

A very important conclusion resulting from Stramska & Petelski's (2003) observations is that whitecap coverage depends on the history of wave field development. They distinguished three sea states, namely, a developed sea, an undeveloped sea and a decreasing sea. In terms of the mechanics of wave generation, all of these states are related to the wind fetch X and wind duration t, or more precisely to non-dimensional quantities such as $\left(\frac{gX}{V_{10}^2}\right)$ or $\left(\frac{gt}{V_{10}}\right)$. As shown in Figure 4, at a given wind velocity V_{10}, fully developed seas (denoted by crosses) are generally characterised by a greater whitecap coverage than undeveloped seas (triangles) and seas corresponding to decreasing winds (diamonds). Fully developed seas occur in regions where the trade winds blow, because there winds vary at smaller time scales. On the other hand, highly variable atmospheric conditions, as in the northern polar regions, result in lower whitecap coverage. The least squares fitting procedure provides

the following relationships (in %) for the whitecap coverage of developed and undeveloped seas (see Figure 4):

$$F_{\mathrm{cov}}^{(\mathrm{dev})} = 0.005 \cdot (V_{10} - 4.47)^3 \tag{16}$$

and

$$F_{\mathrm{cov}}^{(\mathrm{undev})} = 0.00875 \cdot (V_{10} - 6.33)^3. \tag{17}$$

There is no doubt that a correlation between wind speed and whitecap coverage exists, but the premise that whitecap coverage is a function of wind speed alone is unacceptable. Whitecaps are generated by wave breaking; nevertheless, there are many processes that control breaking and the resulting whitecap coverage. Theoretical models based on the various breaking criteria show close links between whitecap coverage and wave breaking probability.

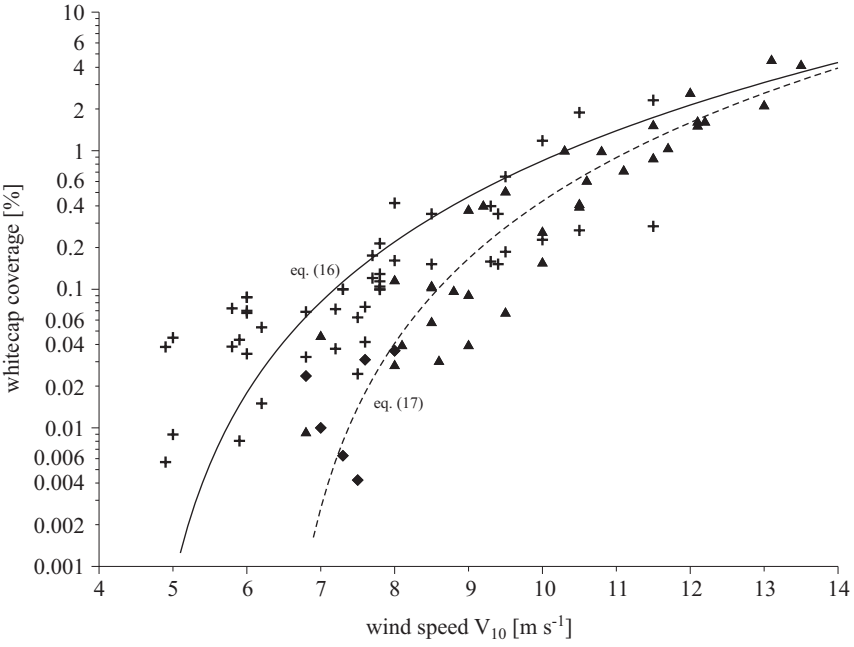

Figure 4. Oceanic whitecap coverage – a function of wind speed in the northern polar waters: crossess – developed sea, triangles – underdeveloped sea, diamonds – decreasing wind (Massel 2007)

2.4.2. Wave breaking criteria and the probability of breaking

Breaking waves are usually associated with steep waves that occur in a given sea. Most descriptions of the breaking phenomenon are still based

on the linear wave theory. This theory provides some convenient measures of incipient wave breaking such as kinematic, geometric and dynamic criteria of wave breaking (Massel 2007). In particular, a wave starts to break when the horizontal fluid velocity at the surface u exceeds the phase velocity C (kinematic criterion). Downstream from this point, fluid particles tend to escape from the water surface.

According to the geometric criteria for breaking to occur, the local surface slope ε_l should exceed some threshold steepness $\varepsilon_{\rm th}$, i.e.

$$\varepsilon_l = \frac{\partial \zeta}{\partial x} \geq \varepsilon_{\rm th}. \tag{18}$$

The spatial fraction of sea surface covered by whitecaps $F_{\rm cov}$, identified with the probability of breaking and characterised by probability density $f(\varepsilon_l)$, becomes

$$F_{\rm cov} \approx F_{br} = \int_{\varepsilon_{\rm th}}^{\infty} f(\varepsilon_l)\, d\varepsilon_l. \tag{19}$$

For wind-induced waves, the probability density of the wave slope $f(\varepsilon_l)$ is given by (Massel 2007):

$$f(\varepsilon_l) = \frac{\varepsilon_l}{\frac{m_4}{g^2}\sqrt{I_c\, I_s}} \exp\left[-\frac{\varepsilon_l^2}{4\frac{m_4}{g^2} I_c\, I_s}\right] I_0\left[\frac{\varepsilon_l^2 (I_c - I_s)}{4\frac{m_4}{g^2} I_c\, I_s}\right], \tag{20}$$

in which $I_0(x)$ is the modified zero-order Bessel function (Abramowitz & Stegun 1975), m_4 is the fourth spectral moment, and the integrals I_c and I_s are

$$I_c = \int_{-\pi}^{\pi} \cos^2\Theta D(\Theta)\, d\Theta, \tag{21}$$

and

$$I_s = \int_{-\pi}^{\pi} \sin^2\Theta D(\Theta)\, d\Theta, \tag{22}$$

in which $D(\Theta)$ is the directionality function of the wave field.

Let us assume that a fully developed sea is characterised by the Pierson-Moskowitz spectrum and spilling breakers predominate. Therefore, using the relationship (19), we obtain (Massel 2007)

$$F_{\rm cov} = \exp\left[-8.265\varepsilon_{\rm th}^2\left(\frac{gX}{V_{10}^2}\right)^{0.22}\right] = \exp\left[-0.5587\left(\frac{gX}{V_{10}^2}\right)^{0.22}\right], \tag{23}$$

where $\varepsilon_{\rm th} = 0.26$.

If the wind fetch in formula (23) is known, $F_{\rm cov}$ becomes a function of wind speed only. This function is shown in Figure 5 for wind fetches

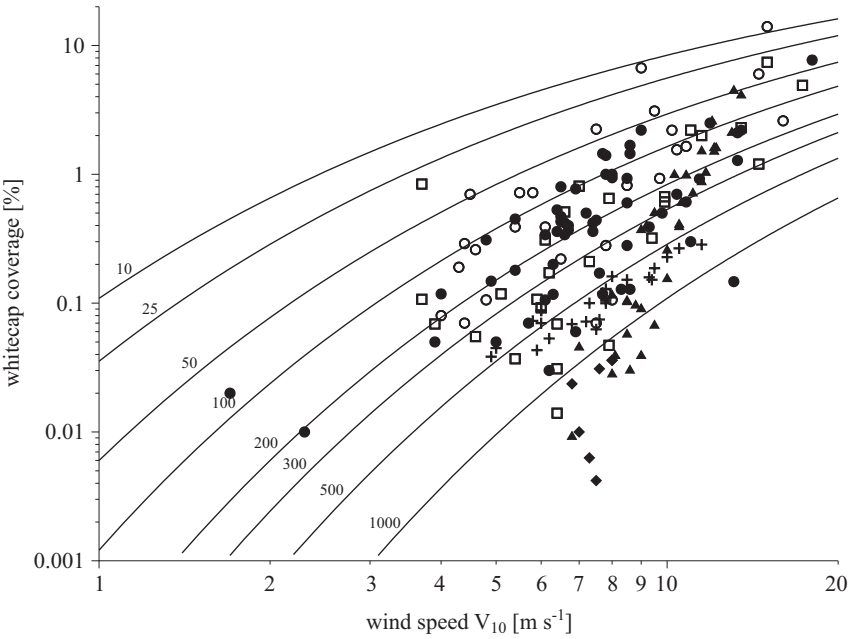

Figure 5. Whitecap coverage, based on the limiting steepness criterion, as a function of wind speed for chosen wind fetches. Experimental data from Monahan & O'Muircheartaigh (1981) and Stramska & Petelski (2003) are added for comparison (Massel 2007)

$X = 10, 25, 50, 100, 200, 300, 500$ and 1000 km. The experimental data, re-analysed by Monahan & O'Muircheartaigh (1981), as well as the data reported by Stramska & Petelski (2003), are given in the same figure. Despite scattering, the computed whitecap coverage provides realistic values under the assumption of an adopted wind fetch range, as the true fetches are unknown. Closer comparison shows that small whitecap coverage appears only for the case of decreasing winds in northern polar waters.

In a simpler way Banner et al. (2000) showed that the probability of breaking increases close to quadratically for so-callled dominant steepness $\varepsilon_d = 1/2 k_p H_d$ when

$$F_{br} = a\,(\varepsilon_d - 0.055)^b, \tag{24}$$

where

$$H_d = 4\left\{\int_{0.7\omega_p}^{1.3\omega_p} S(\omega)d\omega\right\}^{1/2}, \tag{25}$$

in which ω_p and k_p are the frequency and wave number of the spectral peak, a is in the 13.0–37.2 range (mean = 22.0) and b is in the 1.78–2.30

range (mean = 2.01). Massel (2007) showed that when the JONSWAP spectrum is used, the dominant steepness ε_d is related to the wind velocity V_{10} and wind fetch X as follows:

$$\varepsilon_d = a_\gamma \left(\frac{gX}{V_{10}^2} \right)^{-0.11}, \tag{26}$$

where

$$a_\gamma = \begin{cases} 0.1973 & \text{for enhancement parameter } \gamma = 1.0 \\ 0.2661 & \text{for enhancement parameter } \gamma = 3.3 \\ 0.3367 & \text{for enhancement parameter } \gamma = 7.0 \end{cases} \tag{27}$$

Parameter ε_d reflects not only the mean steepness of dominant waves, but also the fundamental role of non-linear group dynamics in determining the onset of breaking.

It is known that near-breaking regular waves have rounded crests with a small radius of curvature, while the vertical downward acceleration at the crest is less than $0.5g$ (it is approximately equal to $0.39g$) (Massel 2007). A distinction should be made between two accelerations of the water particles (Longuet-Higgins 1985). The first acceleration is known as the apparent (or Eulerian) acceleration, $a_z^{(E)} = \partial^2 \zeta(t)/\partial t^2 = \partial w(t)/\partial t$, while the second one, including the convective terms, is known as the real (or Lagrangian) acceleration $a_z^{(L)}$:

$$a_z^{(L)}(x, \zeta, t) = \frac{\partial w}{\partial t} + u \frac{\partial w}{\partial x} + w \frac{\partial w}{\partial z}, \tag{28}$$

in which w is the vertical velocity component at the sea surface. In the linearised theory both acceleration definitions are equal, but in steep waves they are different. To extend this result to the breaking of irregular waves, let us assume that for breaking to occur, the downward acceleration at the crest of the wave should be greater than αg, i.e.

$$\left| \frac{d^2 \zeta}{dt^2} \right| > \alpha g, \tag{29}$$

in which α is a constant. According to Snyder et al. (1983), α varies from 0.4 to 0.52, while the laboratory experiments of Ochi & Tsai (1983) provide the value $\alpha \approx 0.4$.

The starting point for calculating the probability of wave crests breaking in a given wave train is the probability density function of maxima (crests) with a downward acceleration greater than αg. Under the assumption that breaking will occur at a crest point on the sea surface

satisfying condition (29), the probability of wave breaking becomes (Srokosz 1986)

$$F_{br} = \exp\left(-\frac{(\alpha g)^2}{2m_4}\right), \tag{30}$$

where m_4 is the spectral moment of the fourth order. As $m_4 \to \infty$, $F_{br} \to 1$ and the whole surface is covered by whitecaps. It should be noted that the probability F_{br} is independent of any assumption regarding the spectral width, assuming that moment m_4 exists.

To illustrate the dependence of the probability of breaking F_{br} on wind conditions, let us substitute a value for the spectral moment m_4 following from the JONSWAP spectrum. We then obtain the probability of breaking in the form (Massel 2007)

$$F_{br} = \exp\left[-3.858\alpha^2\left(\frac{gX}{V_{10}^2}\right)^{0.22}\right]. \tag{31}$$

The fetch dependence of the probability of breaking is substantial. For a given fetch X, a small value of $\left(\frac{gX}{V_{10}^2}\right)$ is associated with a higher wind velocity and a higher value of the Phillips constant β. The small value of $\left(\frac{gX}{V_{10}^2}\right)$ also provides a high value of ω_p (or small T_p value). This finally yields a higher value of moment m_4 and a higher probability of breaking. Comparison with the experimental data gathered by Xu et al. (2000) in Bohai Bay shows close agreement for the constant $\alpha \approx 0.35$ between the experimental data and the theoretical formula.

2.4.3. Energy dissipation due to wave breaking

Whitecaps are evidence that waves are breaking and energy is being dissipated. However, despite a great research effort, our knowledge of energy dissipation is still fragmentary. This is mostly due to the absence of good quantitative measures of the distribution of breaking and the rates of energy dissipation in breaking waves.

Potentially, energy dissipation could be estimated from the energy budget expressed in wind-wave evolution models. At present, two such approximate methods are considered, namely, the equilibrium range model (Phillips 1985, Hanson & Phillips 1999), and the whitecap model for a fully developed sea (Komen et al. 1984). Tables 2 and 3 list known experimental data and theoretical estimates of energy loss due to breaking. The following notation is used in both tables: C is the dominant phase speed, C_{br} is the phase speed of the breaking waves, θ is the inclination

Table 2. Summary of experimental data on wave energy dissipation due to wave breaking (Massel 2007)

Quantity	Mathematical expression	Source
Number of breaking waves per wave	$N_b = (4.0 \pm 2.0)\times$ $\times 10^{-3}\left(\frac{V_{10}}{C}\right)^3$	Thorpe (1993)
Rate of energy loss per unit surface [J/m^2/s]	$E_{dissrate} = (3.0 \pm 1.8)\times$ $\times 10^{-5}\rho_w\left(\frac{C_{br}}{C}\right)^5 V_{10}^3$	Thorpe (1993)
Rate of energy loss per unit crest length [J/m^2/s]	$E_{dissrate} \sim 0.009\,\rho_w \frac{C_{br}^5}{g\sin\theta}$	Duncan (1981)
	$E_{dissrate} \sim 0.0075\,\rho_w \frac{C_{br}^5}{g\sin\theta}$	Duncan (1983)
	$E_{dissrate} \sim$ $\left(3.2\times 10^{-3} - 1.6\times 10^{-2}\right)\rho_w \frac{C_{br}^5}{g}$	Rapp & Melville (1990)
Rate of total energy dissipation in the equilibrium range [J/m^2/s]	$E_{dissrate} = 4.28\times 10^{-5} V_{10}^{3.74}$	Hanson & Phillips (1990)

Table 3. Summary of theoretical formulae for wave energy dissipation due to wave breaking (Massel 2007).

Quantity	Mathematical expression	Source
Rate of total energy dissipation in the equilibrium range range [J/m^2/s]	$E_{dissrate} = \frac{\gamma_1\rho_w I(3s)}{16[I(s)]^3 g^3}\times$ $\times \int\limits_{\omega_p}^{\infty} \omega^{11} S^3(\omega) d\omega$	Hanson & Phillips (1999)
	$E_{dissrate} = 1.59\rho_w g \frac{m_0 m_2}{m_1}\left(\frac{m_1^4}{g^2 m_0^3}\right)^2$	Komen et al. (1984)
Rate of energy dissipation for an extremely narrow spectrum [J/m^2/s]	$E_{dissrate} = 1.59\rho_w g m_1\left(\frac{m_1^4}{g^2 m_0^3}\right)^2$	Komen et al. (1984)
Energy dissipation for a very narrow spectrum [J/m^2/s]	$E_{diss} = \frac{1}{2}\rho_w g A_{rms}^2 \exp\left(-\frac{A_{br}^2}{A_{rms}^2}\right)$	Longuet-Higgins (1969)
Energy dissipation for a two-dimensional probability density $f(A,T)$ [J/m^2/s]	$E_{diss} = \frac{1}{2}\rho_w g \int\limits_0^{\infty} a_1 I_A(T) dT$	Massel (2007)

of a breaking wave's forward face, m_n is the spectral moment of order n, γ_1 is the numerical constant, $I(s)$ is the spreading function, s is the directional spreading parameter, A_{rms} and A_{br} are the root-mean-square and critical amplitudes respectively, a_1 and $I_A(T)$ are the functions of the period probability density.

For example, in the Phillips equilibrium range model, the whitecapping and the breaking process is assumed to be essentially local in the wave number space. The components with larger wave numbers approach the statistical equilibrium determined by the balance among the input from the wind, wave-wave interactions and energy loss by breaking. If the wave frequency spectra take the form of eq. (13), we obtain the total energy dissipation rate as given in the first integral in Table 3.

The second approach by Komen et al. (1984), also shown in this Table, is in fact an extension of the original model by Hasselmann (1974). In this model the whitecaps are treated as a random distribution of perturbation forces (pressure pulses), of a spatial and temporal scale that is small compared to the wavelength and period of waves. From the physical point of view, it is assumed that the attenuation factor in Hasselmann's model is due to whitecaps situated on the forward faces of waves and to downward pressure on the upward moving water, which results in negative work on the waves. The pressure exerted by the whitecap on the surface of the waves and induced energy decay combined with the attenuation of short waves by the passage of large whitecaps yields the dissipation function in the form (Komen et al. 1984):

$$S_{diss} = C_{diss}\rho g \left(\frac{\hat{\alpha}}{\hat{\alpha}_{PM}}\right)^m \left(\frac{\omega}{\overline{\omega}}\right)^n \overline{\omega} S(\omega), \tag{32}$$

in which C_{diss}, m, and n are fitting parameters, $\overline{\omega}$ is the mean radian frequency and $\hat{\alpha}/\hat{\alpha}_{PM}$ is a measure of the overall steepness of the wave field. It should be noted that for $m = 0$ and $n = 1$, the expression (32) agrees with Hasselmann's (1974) result. Representation of $\hat{\alpha}$ and $\overline{\omega}$ in terms of spectral moments yields the expressions given in Table 2.

Another estimation of energy loss due to breaking for narrow spectra, given in Table 3, results from Longuet-Higgins' (1969) assumption that a given wave breaks in such a way that its energy decreases from some present value to the critical saturation level.

Figure 6 presents an example of the total dissipation rate according to the Phillips model. The set of two lines, corresponding to various fetches, shows almost linear dependence of the total dissipation rate on the wind speed, and very weak influence of the wind fetches. The model results are in satisfactory agreement with experimental data collected in the Gulf of Alaska.

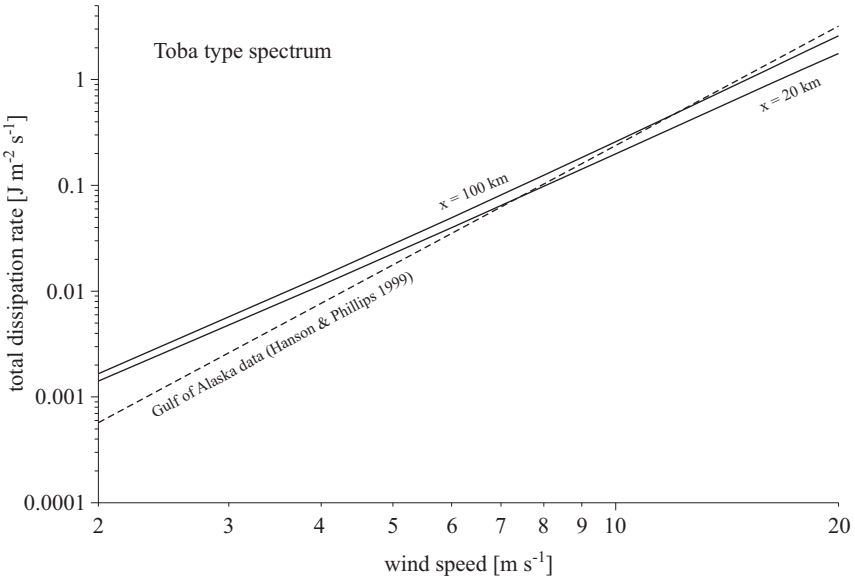

Figure 6. Total dissipation rate as a function of the wind speed according to Phillips (1985) (Massel 2007)

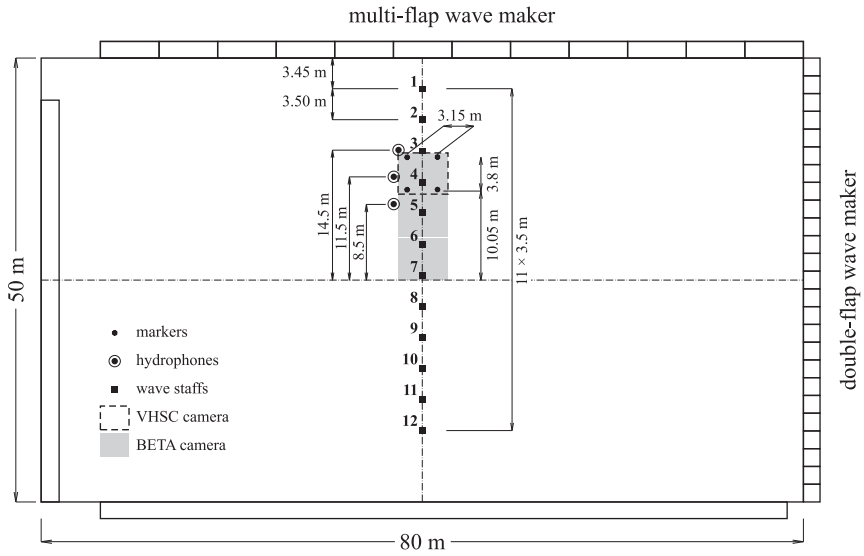

Figure 7. Arrangement of wave gauges in the Ocean Basin (MARINTEK) experiment

Another comparison of observed energy dissipation with results from a narrow spectral model is available from the Ocean Basin Experiment in Trondheim (Norway), where mechanically generated waves were recorded at

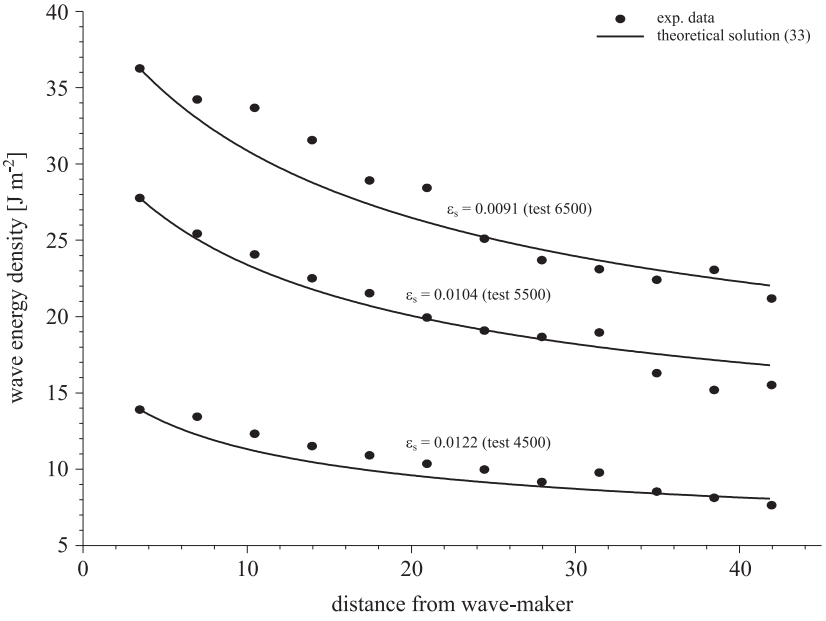

Figure 8. Comparison of the experimental energy attenuation with the theoretical attenuation resulting from Longuet-Higgins' (1969) approach

various points for different values of incident wave steepness (Massel et al. 2001) – see Figure 7.

Using the Longuet-Higgins (1969) solution for the energy dissipation rate (see Table 3), we obtain the following governing equation for the spectral energy density gradient along a distance x (Massel 2007):

$$\frac{dE(x)}{dx} + \frac{\overline{\omega}^2}{2\pi g} E(x) \exp\left(-\frac{b_3}{E(x)}\right) = 0, \tag{33}$$

where

$$b_3 = \frac{1}{2}\rho g \left(\frac{\alpha g}{\omega_{\mathrm{rms}}^2}\right)^2, \tag{34}$$

in which $\overline{\omega}$ is the mean frequency and ω_{rms} is the root-mean-square frequency. Figure 8 compares the wave energy measured at the wave staffs distributed along the main profile during the Ocean Basin Experiment with theoretical results. In all the tests, mechanically generated waves corresponding to the JONSWAP spectrum with enhancement parameter $\gamma = 7.0$ and directional distribution $D(\theta) \approx \cos^2 \Theta$ were used. The initial wave train characteristics were assumed at wave staff 1 located 3.45 m from

the wave generator (see Figure 7). The rate of energy dissipation is shown for three tests of different significant values of wave steepness, where

$$\varepsilon_s = \frac{H_s}{gT_p^2}, \tag{35}$$

in which H_s is the significant wave height.

2.5. Development of extreme waves

In deep water the non-linearities result in focusing of wave energy and therefore in a greater probability of freak wave events. Freak or giant waves correspond to unusually large amplitude waves appearing on the sea surface. Figure 9 shows the time-history of the famous 'New Year wave' about 26 m in height, observed at the Draupner platform in the North Sea on 1 January 1995.

Although various definitions of freak waves have been proposed in the literature, it is usual to characterise a freak wave by its height $H_{\max}$, when $H_{\max}/H_s > 2$ (H_s is the significant wave height), or by the crest height $\zeta_{\max}$, when $\zeta_{\max}/H_s > 1.2$ (Bitner-Gregersen & Hagen 2004). Accordingly, from the Rayleigh distribution it follows that the probability of such extreme wave formation is less than 0.000336 or one wave among more than 2980 waves.

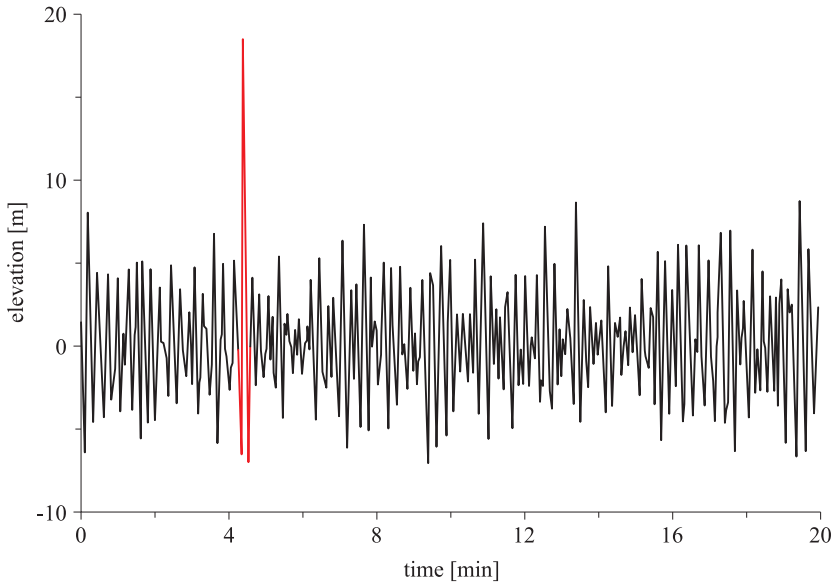

Figure 9. 'The New Year wave' recorded at the Draupner platform in the North Sea on 1 January 1995 (Janssen 2004)

Modelling of special wave events such as extreme, very steep and rapidly varying waves, as well as freak waves and tsunamis, requires a phase-resolving approach. The generation of extreme waves is usually explained by the presence of ocean currents or specific bottom topography, energy focus by refraction or reflection and trapping. However, the question arises as to why exceptionally large waves occur in the open ocean away from non-uniform currents or a special type of bathymetry? During the last 30 years, various mathematical models of freak wave phenomena have been developed and many laboratory experiments conducted, so that great progress has been achieved in the understanding of the physical mechanisms involved (Dysthe 1979, Lo & Mei 1985, Trulsen & Dysthe 1997, Onorato et al. 2000, 2001, 2006, Kharif & Pelinovsky 2003, Kurkin & Pelinovsky 2004, Bitner-Gregersen & Hagen 2004). In particular, the following mechanisms, based on the linear or non-linear description of wave mechanics, are the principal potential sources of extreme wave generation: dispersion enhancement of transient wave groups, spatial focusing of waves, wave-current interaction.

To a first approximation, ocean surface waves can be regarded as narrow spectrum waves when the complex envelope of the sea elevation is described by the non-linear Schrödinger equation (Kharif & Pelinovsky 2003):

$$i\left(\frac{\partial A}{\partial t}+C_g\frac{\partial A}{\partial x}\right)=\frac{\omega_c}{8k_c^2}\frac{\partial^2 A}{\partial x^2}+\frac{\omega_c k_c^2}{2}|A|^2A, \tag{36}$$

in which k_c and ω_c are the wave number and frequency of the carrier wave respectively. The complex amplitude A is a slowly varying function of x and t. These assumptions are physically quite realistic. For example, the above-mentioned 'New Year Wave' had a maximum height of 25.6 m but

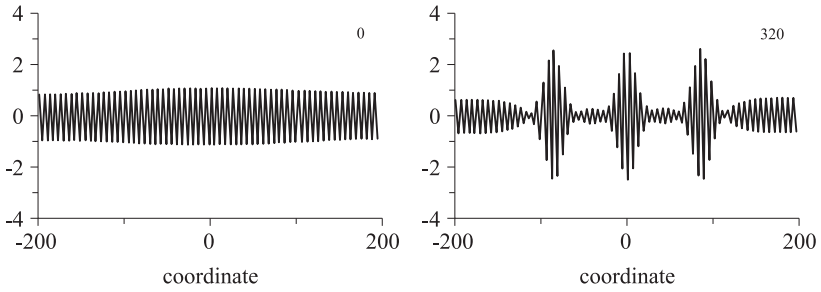

Figure 10. Formation of a highly energetic wave group $\zeta(x)$ in a slowly modulated wave train. The time (0 on the left and 320 on the right) is normalised by the fundamental wave period and the coordinate is in radians of the fundamental mode (Kharif & Pelinovsky 2003)

the envelope of the wave train as a whole was slowly modulated, weakly non-linear and had a relatively small bandwidth. Figure 10 demonstrates that modulational instability leads to the decomposition of an initially homogeneous wave train into a system of envelope quasi-solutions, and that the spatial distribution of wave energy displays significant intermittency.

Since freak waves have a large amplitude and are of short duration, the assumption of weak non-linearity and a narrow-banded spectrum does not correspond exactly to real data. Substantial improvement in the reconstruction of high-amplitude freak waves has been achieved through the extension of weakly non-linear models by the inclusion of higher-order terms of wave steepness, wave-induced mean flow and higher-order linear dispersive terms (Dysthe 1979, Lo & Mei 1985, Trulsen & Dysthe 1996, Dysthe et al. 2003).

In some cases the initial conditions for a numerical simulation are given in the form of frequency spectra, and the so-called time-like non-linear Schrödinger equation is used for analysis. In particular, in terms of the non-dimensional complex amplitude $\tilde{A}$, normalised to the carrier wave amplitude A_c, we have

$$\frac{\partial \tilde{A}}{\partial x} + i\left(\frac{\Delta\omega}{\omega_c}\right)^2 \frac{\partial \tilde{A}}{\partial^2 t} + i\varepsilon^2 \left|\tilde{A}\right|^2 \tilde{A} = 0, \tag{37}$$

in which $\varepsilon = k_c A_c$ is the carrier wave steepness and $1/\Delta\omega$ is the characteristic time scale.

Onorato et al. (2000) reported numerical simulations of the non-linear Schrödinger equation (36) and the Dysthe-Lo-Mei equation (Lo & Mei 1985), which takes the form

$$\frac{\partial \tilde{A}}{\partial x} + i\left(\frac{\Delta\omega}{\omega_c}\right)^2 \frac{\partial \tilde{A}}{\partial^2 t}\frac{\partial \tilde{A}}{\partial^2 t} + i\varepsilon^2 \left|\tilde{A}\right|^2 \tilde{A} + \frac{8\varepsilon^2 \Delta\omega}{\omega_c}\left|\tilde{A}\right|^2 \frac{\partial \tilde{A}}{\partial t} + 4i\varepsilon\left(\frac{\Delta\omega}{\omega_c}\right)^2 \tilde{A}\overline{\frac{\partial \phi}{\partial t}} = 0, \tag{38}$$

This equation is able to account for higher-order physical effects such as the asymmetric evolution of wave packets and side-bands; it also controls the size of the instability region by limiting energy leakage to higher modes. In numerical simulations of the non-linear Schrödinger and Dysthe equations, JONSWAP-type spectra have been used, i.e.

$$S\left(\hat{\omega}\right) = \frac{\beta g^2}{\omega_p^4}\hat{\omega}^{-5} \exp\left(-\frac{5}{4}\hat{\omega}^{-4}\right)\gamma^r, \tag{39}$$

in which $\hat{\omega} = \omega/\omega_p$, γ is the peak enhancement factor of the standard value of 3.3, and function r takes the form

$$r = \exp\left[-\frac{1}{2}\frac{\left(\hat{\omega}-1\right)^2}{\sigma_0^2}\right], \tag{40}$$

where $\sigma_0 = 0.07$ for $\omega < \omega_p$ and $\sigma_0 = 0.09$ for $\omega > \omega_p$. Onorato et al. (2000) showed that the probability density of wave height substantially depends on the enhancement factor γ and on the Phillips constant β. When the coefficients β and γ increase, the effects of non-linearity become more important and freak waves are more likely to occur. For a JONSWAP spectrum with $\beta = 0.0081$ and $\gamma = 6$, simulation using the Dysthe-Lo-Mei equation gives the probability of recording a freak wave five times greater than the one predicted by the Rayleigh distribution. When the linear Schrödinger equation was used in the simulation, no freak waves were found. Moreover, the focusing of frequency modulated wave groups and the blocking effects of spectral components on opposing currents becomes very sensitive to the spectrum width.

Another type of extreme waves are tsunami waves. Tsunami is a Japanese word, in fact a combination of two words: 'ami', which means wave, and 'tsu', which denotes a particular point at the waterline. Thus, a tsunami is 'a wave that approaches the shoreline'. A tsunami is an impulsively driven water wave, caused by the sudden displacement of a large mass of water. The most common cause of such a displacement is a large earthquake, volcanic eruption, landslide either above or below the water surface, or a large meteor impact. Out in the open ocean tsunamis have very long wavelengths and very small amplitudes. They carry enormous energy, and running up onto a shore, their amplitudes can increase very substantially, causing tremendous destruction to populations and structures on shore. On 26 December 2004 a strong tsunami was generated by a magnitude 8.3 earthquake along the Andaman-Sumatra fault. Tsunami waves travelled to every location in the World Ocean. The model by Kowalik et al. (2005) shows that in the Southern Ocean surrounding Antarctica, in the Pacific, and especially in the Atlantic, waves propagate over large distances by energy trapping over oceanic ridges, which causes the amplitude to increase over shallower depths. As the wave speed over a ridge is slower and the wave speed away from a ridge is faster, the joint tsunami wave front is curved in such a way that the energy is directed towards the ridge.

2.6. Steep-wave kinematics

The wave kinematics and loadings due to steep and extreme waves are very important for offshore engineering operations, offshore structures and ship performance. An accurate assessment of the maximum water particle velocities beneath a high wave crest is required for drag force calculations, while the maximum accelerations beneath the steepest section of the wave profile are critical for inertial force calculations. The wave models used to determine the water particle kinematics associated with a measured time

history of the surface elevation $\zeta(t)$ are traditionally based either on a non-linear regular wave theory (for example, a higher-order Stokes' theory) or on an unsteady linear wave theory (a Fourier transform approach).

Gudmestad (1993) provided a comprehensive review of the measured and predicted deep-water kinematics of regular and irregular waves. The main conclusion from his review is that the velocities of regular waves at points below the mean water level are relatively accurately predicted by the non-linear wave theory. However, in random seas and in unsteady sea states, where very steep waves occur, this prediction is not in agreement with experiments, especially near the tip of the waves. In particular, a fifth-order solution suitable for accurately predicting regular waves (Tørum & Gudmestad 1990, Gudmestad 1993) is no longer valid close to the breaking limit for regular waves ($kH/2 \approx 0.44$) and higher-order terms must be included. In the case of random waves, the near-surface velocities beneath a large wave crest are significantly overestimated because the linear theory does not allow individual wave components to ride over one another; rather, all the components oscillate about the still water level.

In recent years, much theoretical and experimental effort has been expended in developing better prediction models for velocities and accelerations. We are particularly interested in the wave characteristics at the wave crest, where the highest velocity and acceleration, as well as wave breaking, are most likely to occur. A full solution of the Laplace equation under periodic lateral boundary conditions is numerically possible but time-consuming. However, we are not usually interested in wave parameters at any time within the wave period. Therefore, it is more useful to concentrate on methodologies that seek only to represent the local (close to the wave crest) behaviour of waves. Moreover, this region coincides with the region of maximum errors in theoretical predictions. To overcome this difficulty, an empirical stretching technique (Wheeler 1970), the best fit of the experimental profile to the fifth-order Stokes profile (Massel 2007) and two alternative local methods for solving irregular wave problems (Sobey 1992, Baldock & Swan 1994) were propounded.

Sobey's (1992) local methodology compromises applicability in a global sense to achieve as exact a representation of wave motion as possible in a local sense. In particular, in his local Fourier approximation methodology, the field equation throughout the fluid domain, the bottom boundary condition at the bed and the free surface boundary conditions at the water surface are satisfied within a window of duration τ, which is small in comparison with the local zero-crossing period. This solution gives an excellent description of the crest kinematics, but is unable to model the

global non-linearities and results in a poor description of the kinematics in the lower layers of the flow.

In contrast to the Sobey model, the method put forward by Baldock & Swan (1994) provides a 'global' solution in the sense that it represents a complete irregular wave record of several waves through the inclusion of both time and space dependence. Thus it can model both local and global non-linearities, but is limited in terms of the total number of Fourier components that can practically be included, resulting in some underestimation of the near-surface kinematics. Also, in certain circumstances, Baldock & Swan's method overestimates the kinematics beneath the still water level. Overall, however, the double Fourier series solution provides both the most accurate and the most reliable estimate of the water particle kinematics for extreme $2D$ waves (Baldock et al. 1996, Smith & Swan 2002).

This is not the case for freak waves and near-breaking waves when the kinematics is not well predicted by any existing theory. A new, fully non-linear unsteady wave model has recently been developed by Clamond & Grue (2001a,b), which offers a substantial improvement in the modelling of steep wave kinematics. The model is based on potential theory and assumes the integration of the kinematic and dynamic boundary conditions at the free surface of very steep (freak) waves. The theoretical results compare favourably with various available sets of experimental data.

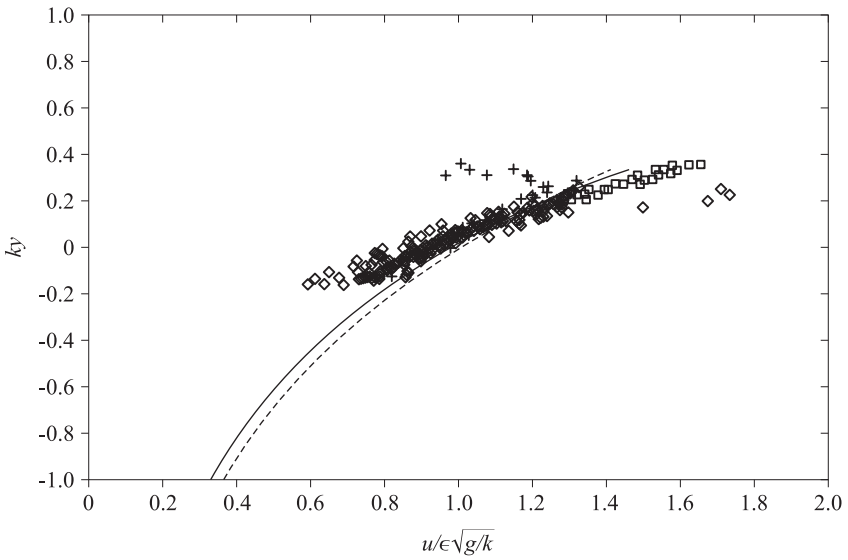

Figure 11. Comparison of experimental velocity profile with theoretical results: solid line – nonlinear solution, broken line – exponential profile (Grue et al. 2003)

Figure 11 compares the experimental velocity profile with the theoretical results of Grue et al. (2003). Measurements and computations show some deep water waves with a fluid velocity up to 75% of the phase speed. The PIV and LDA data demonstrate excellent agreement with the fully non-linear theory. The experimental data correspond to the JONSWAP spectrum with $\omega_p^2 H_s/2g = 0.15$, and the range of the wave slope is $0.21 < \varepsilon < 0.34$. These data are compared to the non-linear computations with steepness $\varepsilon = 0.29$. A surprising result is that the exponential profile e^{ky} compares well with all measurements in deep water.

Accelerations at the sea surface are required to estimate the inertia forces on offshore installations. Very few measurements exist of the real acceleration below steep waves (see, for example, Bonmarin & Kjeldsen 2000, Grue & Jensen 2006). In particular, Grue and Jensen reported a maximum negative vertical acceleration at the wave crest of about $1.1g$, while the upward vertical acceleration grows to about $1.5g$ in the front face of the wave at the base below the overturning jet of the plunging breakers. The fully non-linear theoretical model for accelerations in unsteady waves shows very good agreement with experiments. It was shown that the convective term is of the same order of magnitude and of opposite sign to the local acceleration, and it cannot be neglected when estimating the acceleration and forces (Jensen et al. 2007).

2.7. Dependence of aerosol fluxes on wave breaking conditions

All non-gaseous particles suspended in the atmosphere are called aerosols. Aerosols are composed mainly of droplets and crystals but also of organic matter particles and large ions. These constituents can be both natural and anthropogenic: liquid seawater drops, dry sea salt particles, dust transport from the deserts by wind, as well as particles resulting from human activities related to industrial processes and agriculture, volcanic eruptions, and meteorite destruction in the atmosphere. Aerosol emission from the global ocean is one of the major natural sources of aerosols in the atmosphere. Because approximately 71% of the Earth's surface is covered by oceans, marine aerosols play an important role in various geochemical and geophysical processes and in the Earth's climate as a whole. It is estimated that the annual production of marigenic aerosols varies from 0.3×10^{12} kg to 30×10^{12} kg, corresponding to a sea aerosol mass flux over the oceans of $0.03 \times 10^{-3}\,\mathrm{kg\,m^{-2}\,s^{-1}}$ to $3 \times 10^{-3}\,\mathrm{kg\,m^{-2}\,s^{-1}}$ (Lewis & Schwartz 2004).

The marine aerosol generation functions depend on the product of the so-called size-dependent production flux $f_{\mathrm{prod}}^{(\mathrm{wc})}(r)$ and whitecap coverage

Table 4. Monthly sea salt production ($\times 10^6$ kg) in the Baltic Sea in 1999 (Massel 2007)

Month	Criterion for determination of whitecap coverage	
	limiting steepness	limiting vertical acceleration
January	1.39	4.87
February	3.11	8.28
March	0.68	3.07
April	0.62	2.96
May	0.15	1.13
June	0.09	0.69
July	0.17	1.23
August	0.06	0.61
September	0.26	1.60
October	1.70	5.83
November	3.37	8.66
December	7.97	14.96

F_{cov}. The production flux $f_{\mathrm{prod}}^{(\mathrm{wc})}(r)$ is only a function of radius r, while the whitecap coverage F_{cov} depends on the rate of energy dissipation and sea state. Therefore seasonal wind and wave data for a given sea basin provide an opportunity to estimate the aerosol production there. For example, Table 4 summarises the monthly sea salt production for 1999 in the Baltic Sea. Sea salt production is highest during winter and lowest during summer. Taking into account the fact that the surface area of the Baltic Sea is about 384 700 km^2, the monthly average sea salt production per km^2 is 20.72–38.90 kg during stormy weather.

This estimate of sea salt production is based on the assumption that the whitecap coverage is parameterised in terms of the sea state parameters through two wave breaking criteria, i.e. the limiting steepness and the limiting vertical acceleration. The table indicates that sea salt production based on the limiting vertical acceleration criterion is higher than that calculated using the limiting steepness criterion. In particular, during the winter months, the ratio of both production rates is about 2 and for smaller waves in summer, the difference between the methods of calculation is even greater.

3. Waves in shallow waters

3.1. Action balance equation components for shallow water

Present-day coastal engineering projects are becoming more complex, and advanced near-shore wave models are required to provide results of

greater accuracy. In particular, design calculations are needed to assess the applied water loading on structures, the stability and transport of bed material, and the run-up on beaches and over-topping of breakwaters. The great accuracy of models requires the formulation of predictive models in which non-linearities and the unsteady character of the wave field are both taken into account.

Predictive models in shallow waters are based on the action balance equation, similar to eq. (1). In Cartesian co–ordinates we have (Holthuijsen 2007)

$$\frac{\partial N}{\partial t} + \frac{\partial [C_{g,x}\, N]}{\partial x} + \frac{\partial [C_{g,y}\, N]}{\partial y} + \frac{\partial [C_\theta\, N]}{\partial \theta} + \frac{\partial [C_\sigma\, N]}{\partial \sigma} = S, \tag{41}$$

in which $C_{g,x}$ and $C_{g,y}$ are group velocities in x- and y-space respectively. The fourth term, with phase velocity C_θ in θ-space, represents depth-induced and current-induced refraction. The fifth term is the shifting of the frequency due to variation in depth and currents with phase velocity C_σ in σ-space. In shallow water, the source term S includes generation by wind, non-linear wave-wave interaction (triad interaction), energy dissipation due to wave breaking and bottom friction.

In shallow water a transfer of energy takes place from two primary waves to a third wave, through the near-resonant triad interactions, in contrast to the quadruplet wave-wave interactions in deep waters. The necessary requirements are that the sum of the frequencies and the vector wave numbers of the interacting waves must be (nearly) zero (Massel 1996), i.e.

$$\omega_1 \pm \omega_2 \pm \omega_3 = 0 \tag{42}$$

and

$$\mathbf{k}_1 \pm \mathbf{k}_2 \pm \mathbf{k}_3 = \mathbf{k}_\delta \tag{43}$$

The mismatch in the wave number $\mathbf{k}_\delta$ approaches zero only for extremely shallow water, where waves are non-dispersive.

In sea waters of limited depth with a sandy bottom, bottom friction is the dominant mechanism for dissipation. This mechanism covers the complicated processes in the relatively thin turbulent layer at the bottom. Using the quadratic law to estimate the shear stress at the bottom, the energy-dissipation rate for random waves becomes (Collins 1972)

$$D_{fr} = -\rho_w C_{fr} u^2_{rms,bottom} \cdot u_{rms,bottom}, \tag{44}$$

in which $u_{rms,bottom}$ is the root-mean-square orbital velocity at the bottom.

In general, if an accurate description of water particle kinematics and dynamics is required, in particular close to the water surface, then the wave models applied must incorporate both the non-linearity and unsteadiness of events. Some recent theoretical developments in single frequency wave

mechanics for constant as well as for varying water depths are discussed in some detail in the following Sections.

3.2. Waves in waters of constant depth

In waters of intermediate depths the water particle kinematics and dynamics, corresponding to a measured or predicted time-history of surface elevation $\zeta(t)$, are usually determined according to Stokes' non-linear steady wave theory (Fenton 1985), while in very shallow waters of constant depth, a non-linear cnoidal theory is more appropriate (Fenton 1979). In linear models, the unsteadiness and irregular nature of surface waves may be included, but the non-linearity is not. The observed surface elevation is assumed to be the sum of freely propagating wave components, each of which satisfies the linear dispersion relation. However, this type of solution, particularly for near-surface velocities, results in significant errors due to high frequency contamination.

For non-linear and unsteady surface waves Longuet-Higgins & Cokelet (1976) in their pioneer study developed an exact method for extreme $2D$ waves. They showed that the non-linear free surface conditions can be re-arranged in such a way that a spatial representation of surface elevation and velocity potential Φ are defined at some initial time $t = t_0$, and the entire solution can be time-matched to give values for $\zeta(x)$ and $\Phi(\zeta, x)$ at all subsequent times. This procedure was extended by Dold & Peregrine (1984) for a spatially periodic wave field with no restriction on the water depth. First, they considered six laboratory tests with different periods, corresponding to deep, intermediate and shallow water conditions, and two spectra – a broad-banded spectrum and a narrow-banded spectrum. These tests were successfully reproduced by Dold and Peregrine's numerical model for adopted initial conditions. Subsequently, Smith and Swan (2002) used these exact numerical calculations rather than laboratory data as benchmark data to compare numerical results with other prediction models. These comparisons indicate that the fifth-order Stokes' solution or linear random wave theory provides a poor description of water particle kinematics as it is unable to model the unsteadiness and the non-linearities that are common in extreme wave events. On the other hand, the local Fourier series solution (Sobey 1992) and the double Fourier series (Baldock & Swan 1994) mentioned above provide improved representations of the surface profile and wave kinematics, also for waves propagating in finite water depths.

Fenton (1986) developed an alternative local approximation method for unsteady waves in shallow water. In this method, the local solution is represented by a truncated polynomial series for the complex potential function. The unknown polynomial terms are determined numerically to

fit the non-linear free surface conditions using a measured time history of the surface elevation. This procedure is best suited for long waves where the vertical variation in the fluid velocities can be described by a polynomial function.

3.3. Wave propagation over gradually varying water depths

Propagation of surface waves over a bottom of varying depth is a mathematically difficult problem. Therefore, although the non-linear effects become significant close to the shoreline, a linear solution is still very useful, and approximate wave models retaining only the essential features of the problem are used. If relative wave height and bottom slope are small, non-linearities are weak, the mild-slope equation developed by Berkhoff (1972) and many of its alternative derivations and numerous extensions provide effective tools to predict wave variation in regions of moderate size. In all these solutions, the vertical structure of the wave potential is predetermined.

According to Booij (1983), the mild-slope equation gives accurate results even with a plane bottom slope up to 1:3. However, steep bottom slopes, such as underwater shoals and coral reefs (Lie & Tørum 1991, Massel 1993, 1996) require the inclusion of higher-order terms and possibly wave breaking mechanisms in the mild-slope equation for the wave amplitude A variation:

$$\frac{d^2A}{dx^2} + (CC_g)^{-1}\frac{d(CC_g)}{dx}\frac{dA}{dx} + [k^2(1+\psi) + i\gamma k]A = 0, \tag{45}$$

in which

$$\psi = E_1(kh)\left(\frac{dh}{dx}\right)^2 + E_2(kh)\frac{g}{\omega^2}\frac{d^2h}{dx^2}, \tag{46}$$

and $\gamma = \gamma_{br} + \gamma_{fr}$. The ψ term describes the influence of bottom slope dh/dx and bottom shape d^2h/dx^2, and the γ term represents the sum of energy dissipated due to wave breaking γ_{br} and bottom friction γ_{fr}, and E_1 and E_2 are functions of non-dimensional water depth (Massel 1996).

The modelling of energy dissipation due to breaking in the wave train, is usually based on four main assumptions:

- dissipation is equivalent to dissipation in a bore connecting two regions of uniform flow (Battjes & Janssen 1978),
- dissipation is proportional to the difference between the local energy flux and the stable energy flux (Dally et al. 1985),
- the breaking wave height is saturated, i.e. the wave height is proportional to the local water depth and the proportionality coefficient is assumed to be constant across the surf zone,
- dissipation is controlled by the presence of a surface roller (Svendsen 1984).

For example, using the first approach, the quantity γ_{br} becomes (Massel 1996)

$$\gamma_{br} = \frac{3\alpha_0\omega_p}{4\sqrt{\pi}} \frac{\sqrt{gh}}{CC_g} \frac{H_{rms}}{h} \left(\frac{H_{rms}}{\Gamma h}\right)^4, \tag{47}$$

in which H_{rms} is the root-mean-square wave height, ω_p is the peak frequency, α_0 is a coefficient of $O(1)$ and $\Gamma \approx 0.3$–0.5.

The rate of energy dissipation due to bottom friction γ_{fr} is given by (Massel 1996):

$$\gamma_{fr} = \frac{16C_{fr}}{3\pi} \frac{u_{bottom}^3}{gC_gH_{rms}^2}. \tag{48}$$

where C_{fr} is the friction factor, and u_{bottom} is the velocity amplitude at the bed.

In recent years, many papers on the applicability of the mild-slope equation to coastal problems have been published. For example, the extended refraction-diffraction equation has been applied to predict wave transformation and breaking as well as a wave-induced set-up on two-dimensional reef profiles of various shapes (Massel & Gourlay 2000). Comparison of predicted and observed wave heights and set-up values showed good agreement.

However, equation (45) does not satisfy exactly the Neumann condition on a sloping bottom. This means that the velocity field in the vicinity of the bottom is poorly represented and wave energy is not generally conserved. In order to improve the mild-slope representation in the bottom layer, Athanassoulis & Belibassakis (1999) developed the consistent coupled-mode theory, in which an additional term, called the sloping-bottom mode, was introduced to satisfy the bottom condition exactly. The equation for wave amplitude A then takes the form

$$A(x,z) = A_{-1}(x)\cdot Z_{-1}(z,x) + A_0(x)\cdot Z_0(z,x) + \sum_{n=1}^{\infty} A_n(x)\cdot Z_n(z,x), \tag{49}$$

where $A_0(x)$ $Z_0(z,x)$ denotes the propagating mode, and the remaining terms $A_n(x)$ $Z_n(z,x)$ are the evanescent modes. The functions $Z_0(z,x)$ and $Z_n(z,x)$ are the classical functions representing the z-dependence of wave motion for propagating and evanescent modes respectively. The additional sloping-bottom mode $A_{-1}(x)$ $Z_{-1}(z,x)$ provides a proper Neumann condition over a non-horizontal bottom when the function $Z_{-1}(z,x)$ takes the form

$$Z_{-1}(z,x) = h(x)\left[\left(\frac{z}{h(x)}\right)^3 + \left(\frac{z}{h(x)}\right)^2\right]. \tag{50}$$

This idea was further extended to a $3D$ environment (Belibassakis et al. 2001) and to second-order Stokes waves over variable bathymetry (Belibassakis & Athanassoulis 2002). By way of example, Figure 12 presents the resulting equipotential lines (real and imaginary parts) when 6 evanescent modes are included. Now we can see that the equipotential lines intersect the bottom profile perpendicularly.

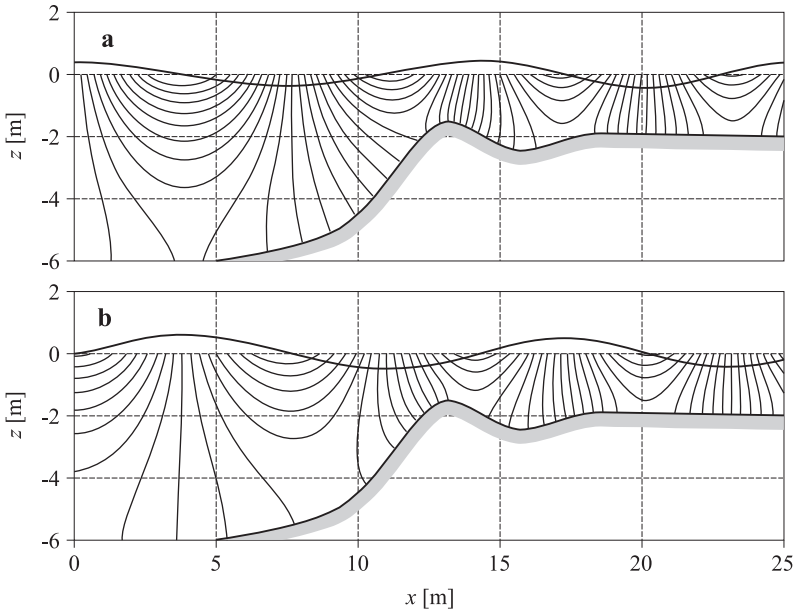

Figure 12. Equipotential lines for wave motion over topography: a) real part of the potential, b) imaginary part of the potential (Athanassoulis & Belibassakis 1999)

3.4. Run-up of waves at a beach and wave-induced groundwater circulation

3.4.1. Waves on beaches

Sandy beaches are highly exploited but very dynamic and fragile environments. The beach system is driven largely by the physical energy induced by waves and tides. In tideless seas, the flow is totally controlled by the dynamics of surface waves on the beach. Wave motion on beaches is very complex and the groundwater flow is different in different beach regions. In Region 3, (see Figure 13), the wave run-up contributes mainly to the raising of the coastal water table. On the other hand, the beach groundwater flow in the set-up region induces a groundwater circulation that contributes to the submarine groundwater discharge.

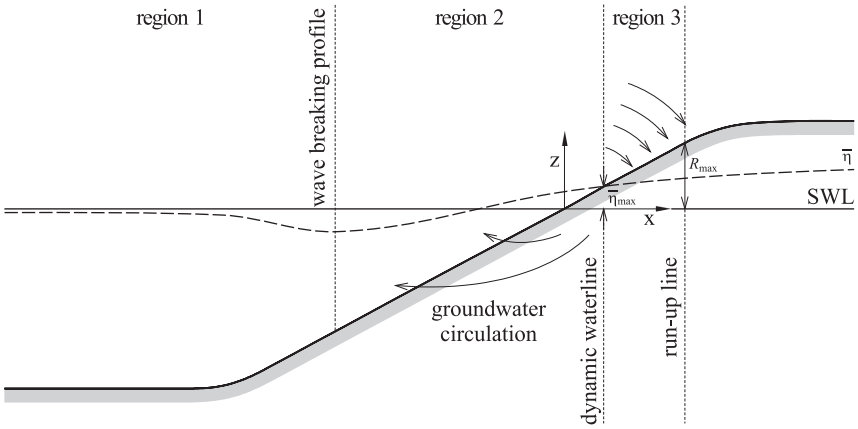

Figure 13. Reference scheme and relationships between wave run-up, infiltration and coastal watertable (Massel & Pelinovsky 2001)

Propagating waves transport not only energy but also momentum, which is a vector quantity. The transport of momentum is equivalent to a stress and known as radiation stress (Longuet-Higgins & Stewart 1964). As waves propagate towards the shore, they become steeper as the water depth becomes shallower; at a certain depth they lose their stability and finally start to break. When waves break, wave energy is dissipated and the radiation stress is reduced, which gives rise to changes in the mean sea level (MSL). The balance of the sea level gradient and the gradient of radiation stress takes the form

$$\frac{dS_{xx}}{dx} + \rho g \left(h + \overline{\eta}\right) \frac{d\overline{\eta}}{dx} = 0, \tag{51}$$

in which $\overline{\eta}$ is the change of MSL due to wave action, and S_{xx} is the radiation stress tensor component. The change of $\overline{\eta}$ due to wave action is shown schematically in Figure 13. For water depth decreasing monotonically towards the beach, the maximum set-down of $\overline{\eta}_{br} = -1/16 H_{br}^2/h_{br}$ appears close to the breaking point, while the maximum set-up $\overline{\eta}_{\max} = 5/16 H_{br}^2/h_{br}$ occurs at the dynamic waterline. The set-up depends on the incoming wave height. Thus, for a stationary situation, the set-up is stationary. However, the waves usually arrive in a group, which causes the set-up to fluctuate.

The wave run-up height $R_{\max}$ is defined here as the maximum vertical height above still water level reached by the wave uprush. The run-up height is always greater than the wave set-up. On the other hand, wave run-down is defined as the lowest vertical height reached by the backwash of a wave before the uprush of the next wave starts to run-up the beach face.

The wave run-up limit and induced water infiltration into a beach body is a response to the instantaneous flow of the surface water. Therefore, modelling the surface oscillation should be based on the phase-resolving wave type model. Available run-up models usually assume that waves are non-dispersive and that the phase velocity depends on the water depth only (Carrier & Greenspan 1958, Pelinovsky 1996). This assumption is applicable to tsunami and wind-induced waves very close to the shoreline.

However, in deeper water, waves are usually dispersive. Thus, we need an approach in which the dispersive character of waves is maintained seawards and the approximation of shallow water is used close to the waterline. Massel & Pelinovsky (2001) attempted to develop a more complex approach for the run-up of dispersive breaking and on-breaking waves. Waves approaching the shallow water area were modelled by the mild-slope equation. At very small water depths, the non-linear and linear equations for shallow water waves are considered and the dissipation due to wave breaking is included, providing a more realistic estimation of run-up characteristics. For long, non-dispersive waves, the governing equations are usually based on the Carrier & Greenspan (1958) transformation and its various modifications (Pelinovsky 1996, Belibassakis & Athanassoulis 2006).

In the simple case when a plane slope merges into a horizontal bottom, the surface elevation $\zeta(x,t)$ over the sloping bottom takes the form

$$\zeta(x,t) = \Re\frac{H_i}{2} K_T\, J_0\left[\sqrt{\left(1+\frac{iD_b}{\omega}\right)\frac{4\omega^2(-x)}{g\beta_1}}\right]\exp(-i\omega t), \tag{52}$$

in which H_i is the incident wave height, K_T is the transmission coefficient of wave motion from the horizontal bottom region to the sloping bed region β_1 is the beach slope, D_b is the dissipation factor due to wave breaking and $J_0(x)$ is a zero-order Bessel function of the first kind. The transmission coefficient K_T becomes

$$K_T = \frac{2}{J_0(\epsilon) - i\sqrt{1+i\frac{D_b}{\omega}}J_1(\epsilon)}, \tag{53}$$

in which

$$\epsilon = \sqrt{\left(1+\frac{iD_b}{\omega}\right)\frac{4\omega^2(-x)}{g\beta}}. \tag{54}$$

The values of run-up, observed in the experiments, also include the set-up mechanism. Therefore, the final maximum run-up height becomes

$$R_{\max} = \frac{H_i}{2} \mid K_T \mid + \overline{\eta}_{\max}, \tag{55}$$

where $\overline{\eta}_{\max}$ is the solution of eq. (51).

The experimental data on wave run-up are numerous and some comparisons between experiments and theory can be found Massel & Pelinovsky (2001).

Another convenient method of treating the problem of wave motion in a plane-beach (wedge) region was published recently by Belibassakis & Athanassoulis (2006), who used cylindrical-polar coordinates ($x = r\cos\theta$, $z = r\sin\theta$) in the vertical plane with the origin at the waterline. If we ignore the evanescent modes, the governing equation for the wave amplitude $A(r)$, close to the waterline ($r \to 0$) has the form

$$\frac{\partial^2 A}{\partial r^2} + \frac{1}{r}\frac{\partial A}{\partial r} + \frac{1}{r}\left(\frac{\mu}{\theta} - \frac{\mu\theta}{3}\right) A = 0, \tag{56}$$

where $\mu = \omega^2/g$ and $h = -r\sin\beta_1$.

Belibassakis and Athanassoulis showed that the solution of the above equation is in agreement with that of equation (51). This solution is sometimes used as the initial value for solving the more complex problem of wave propagation over a sloping sea bottom.

3.4.2. Wave-induced groundwater circulation

Water flow through the beach body is of great importance for introducing water, organic materials and oxygen to the ground environment, as well as for sediment transport, coastal structure stability and modern beach nourishment techniques. Water flow controls the vertical and horizontal, chemical and biological gradients, and nutrient exchange in the beach, which helps to maintain biological activity in the porous media. This provides a basis for assessing the vulnerability of a beach's biodiversity and the functioning of the interaction between tourism, natural changes and the physical properties of the sea in such an ecosystem (Węsławski et al. 2000).

As it is diffcult to estimate the infiltration of water into beach sand under real sea conditions, a controlled, almost full-scale experiment was carried out in the Large Wave Channel in Hanover (Germany) (Massel et al. 2004, 2005). During the experiment, a water depth of 4 m in front of the beach was assumed. Natural beach sand with fine-grained sand of mean diameter $D_{50} = 0.24\,\mathrm{mm}$ was used and a uniform beach with a 1/20 slope was created in the channel. To measure the pore water pressure, four systems of pressure gauges were installed along the beach face. In each system, four piezoelectric pressure sensors were fixed to a metal rod arranged in the form of a cross. Such an arrangement enables not only the pore pressure to be estimated, but also the horizontal and vertical water velocities in the beach body through the simultaneous measurements of pore pressures.

The experiment revealed the dual nature of the recorded pore pressures. Beyond the breaker zone, only the rapidly-varying phase-resolving pore pressure component due to surface variation is observed, while within the surf zone, the phase-resolving component as well as the slowly varying phase-averaged pore pressure component due to wave set-up were present (Massel 2001, Massel et al. 2004, 2005).

To explain the nature of the rapidly varying pore-pressure component and the resulting velocity circulation, an exact close-form solution based on the Biot theory for multiphase flow has been developed. This solution takes into account soil deformations, volume change and pore-water pressure. When the stiffness ratio $G/E'_w \geq 100$ (G is the shear modulus of the soil and, E'_w is the apparent bulk modulus of the pore water), the vertical distribution of the pore pressure is very close to the Moshagen & Tørum (1975) solution assuming that the soil is rigid and the fluid compressible.

The apparent bulk modulus depends on the degree of saturation by air, which is very difficult to estimate under experimental conditions. Extensive field measurements carried out by de Rouck & Troch (2002) showed that there was approximately 3% gas in the soil pores. Tørum (2007) argued that in laboratory conditions, the air/gas content can be in the range 3–10%.

Figure 14 compares the theoretical results with the Large Wave Channel experimental tests (Massel et al. 2005). It shows the long-wave case

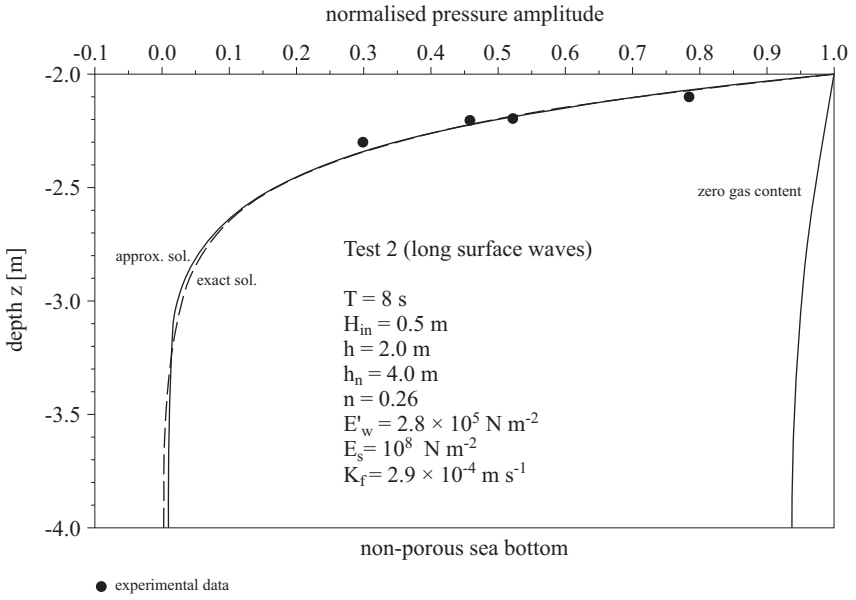

Figure 14. Comparison between experimental and theoretical values of pore pressure (Massel et al. 2005)

and three solutions, namely the exact closed-form solution, the Moshagen & Tørum (1975) solution and the special case of a rigid soil and incompressible water. The solution for a partly saturated soil, when $G/E'_w \to \infty$, is very close to the exact solution and compares well with the experimental data.

The radiation stress tensor S_{xx} induces a change in the mean water level that exhibits two different horizontal steady pressure gradients. These steady pressure gradients induce two systems of pore water circulation, related to the signs of different gradients (Massel 2001). For the offshore gradient, the horizontal excess pressure carries the flow in the offshore direction. However, closer to the shore, the pressure gradient is reversed and the resulting flow moves shorewards. The final circulation pattern due to wave run-up on a porous beach is the result of the combined impact of the phase-resolving and phase-averaged pore pressure components.

4. Conclusions

This overview examines the role that ocean waves play in the interactions of atmosphere and ocean. In particular, it is demonstrated that ocean waves evolve in space and in time according to the well-known energy balance equation. This equation is the basis for modern wave forecasting techniques. Although these techniques have not been discussed in the review, it should be stressed that significant improvements in wave forecasting have been made in the last ten years. To a large extent this is related to substantial progess in the description of wind forcing and other processes, as well as to the more efficient use of satellite observations and assimilation methods.

An observation that strikes one when reviewing the modelling techniques of surface wave propagation is the increasing variety and complexity of models in which more physical processes are included, greater precision and resolution are achieved and extended ranges of applicability are demonstrated. In particular, substantial progress has been made in the modelling of freak and tsunami waves. Estimated velocities and the forces induced by these events can help improve the design of ships and offshore structures.

In coastal waters, more processes have to be taken into account than in oceanic waters. The modified mild-slope equation approach offers a more accurate description of wave propagation over a sloping bed. However, highly non-linear phenomena such as wave breaking and wave run-up require new theoretical ideas and more precise experimental data. In general, the selection of any model should be based on a proper appreciation of the physical processes to be modelled. Finally, in order to estimate the applicability of particular models, comparison with high quality

experimental data, collected in nature or under laboratory conditions, is necessary.

Acknowledgements

The author would like to thank the anonymous reviewers for their very helpful suggestions and improvements to this paper.

References

Abramowitz M., Stegun I. A., 1975, *Handbook of mathematical functions*, Dover Publ., New York, 1045 pp.

Athanassoulis G. A., Belibassakis K. A., 1999, *A consistent coupled-mode theory for the propagation of small-amplitude water waves over variable bathymetry regions*, J. Fluid Mech., 389, 275–301.

Baldock T. E., Swan C., 1994, *Numerical calculations of large transient water waves*, Appl. Ocean Res., 16 (2), 101–112.

Baldock T. E., Swan C., Taylor P. H., 1996, *A laboratory study of non-linear surface waves on water*, Philos. T. Roy. Soc. A, 354 (1707), 1–28.

Banner M. L., Babanin A. V., Young I. R., 2000, *Breaking probability for dominant waves on the sea surface*, J. Phys. Oceanogr., 30 (12), 3145–3160.

Banner M. L., Song J. B., 2002, *On determining the onset and strength of breaking for deep water waves. Part II: Influence of wind forcing and surface shear*, J. Phys. Oceanogr., 32 (9), 2559–2570.

Battjes J. A., Jansen J. P. F. M., 1978, *Energy loss and set-up due to breaking of random waves*, Proc. 16th Coastal Eng. Conf., 1, 563–587.

Belibassakis K. A., Athanassoulis G. A., 2002, *Extension of second-order Stokes theory to variable bathymetry*, J. Fluid Mech., 464, 35–80.

Belibassakis K. A., Athanassoulis G. A., 2006, *A coupled-mode technique for the run-up of non-breaking dispersive waves on plane beaches*, Proc. 25th Int. Conf. Offshore Mech. Arctic Eng., OMAE 2006 – 92162, 1–8.

Belibassakis K. A., Athanassoulis G. A., Gerostathis T. P., 2001, *A coupled-mode model for the refraction-diffraction of linear waves over steep three-dimensional bathymetry*, Appl. Ocean Res., 23 (6), 319–336.

Benjamin T. B., 1967, *Instability of periodic wavetrains in nonlinear dispersive systems*, P. Roy. Soc. Lond. A Mat., 299 (1456), 59–76.

Benjamin T. B., Feir J. E., 1967, *The disintegration of wave trains in deep water. Part 1. Theory*, J. Fluid Mech., 27 (3), 417–430.

Berkhoff J. C. W., 1972, *Computation of combined refraction-diffraction*, Proc. 13th Coastal Eng. Conf., 1, 471–490.

Bitner-Gregersen E. M., Hagen Ø., 2004, *Freak wave events within the second order wave model*, Proc. 23rd Int. Conf. Offshore Mech. Arctic Eng., OMAE 2004 – 51410.

Bonmarin P., Kjeldsen P., 2000, *Some geometric and kinematic properties of breaking waves*, [in:] *Rogue waves 2000*, M. Olagnon & G. A. Athanassoulis (eds.), Edn. Ifremer, Brest, 169–180.

Booij N., 1983, *A note on the accuracy of the mild-slope equation*, Coast. Eng., 7 (3), 191–203.

Bretherton F. P., Garrett C. J. R., 1969, *Wave trains in inhomogeneous moving media*, P. Roy. Soc. Lond. A Mat., 302 (1471), 529–554.

Carrier G. F., Greenspan H. P., 1958, *Water waves of finite amplitude on a sloping beach*, J. Fluid Mech., 4 (1), 97–109.

Clamond D., Grue J., 2001a, *A fast method for fully non-linear water-wave computations*, J. Fluid Mech., 447, 337–355.

Clamond D., Grue J., 2001b, *On efficient numerical simulations of freak waves*, Proc. 11th Int. Offshore Polar Eng. Conf.

Collins J. I., 1972, *Prediction of shallow-water spectra*, J. Geophys. Res., 77 (15), 2693–2707.

Dally W. R., Dean R. G., Dalrymple R. A., 1985, *Wave height variation across beaches of arbitrary profile*, J. Geophys. Res., 90 (C6), 11 917–11 927.

Davidan I. N., Lopatukhin L. I., Rozkhov W. A., 1978, *Wind waves as random hydrodynamic process*, Gidrometeoizdat, Leningrad, 287 pp., (in Russian).

Davidan I. N., Lopatukhin L. I., Rozkhov W. A., 1985, *Wind waves in World Ocean*, Gidrometeoizdat, Leningrad, 254 pp., (in Russian).

Dean R. G., Dalrymple R. A., 1998, *Water wave mechanics for engineers and scientists*, Adv. Ser. Ocean Eng., Vol. 2, World Sci. Publ., Singapore, 353 pp.

de Rouck J., Troch P., 2002, *Pore water pressure response due to tides and waves based on prototype measurements*, PIANC Bull., 110, 9–31.

Dold J. W., Peregrine D. H., 1984, *Steep unsteady waves: an efficient computational scheme*, Proc. 19th Int. Conf. Coastal Eng., 1, 955–967.

Dold J. W., Peregrine D. H., 1986, *Water-wave modulation*, Proc. 20th Int. Conf. Coastal Eng., 1, 163–175.

Duncan J. H., 1981, *An investigation of breaking waves produced by a towed hydrofoil*, P. Roy. Soc. Lond. A Mat., 377 (1770), 331–348.

Duncan J. H., 1983, *The breaking and non-breaking wave resistance of a two-dimensional hydrofoil*, J. Fluid Mech., 126, 507–520.

Dysthe K. B., 1979, *Note on a modification to the non-linear Schrödinger equation for application to deep water waves*, P. Roy. Soc. Lond. A Mat., 369 (1736), 105–114.

Dysthe K. B., Trulsen K., Krogstad H. E., Socquet-Juglard H., 2003, *Evolution of a narrow-band spectrum of random surface gravity waves*, J. Fluid Mech., 478, 1–10.

Fenton J. D., 1979, *A high-order cnoidal wave theory*, J. Fluid Mech., 94 (1), 129–161.

Fenton J. D., 1985, *A fifth order Stokes' theory for steady waves*, J. Waterw. Port C. Div., 111 (2), 216–234.

Fenton J. D., 1986, *Polynomial approximation and water waves*, Proc. 20th Coastal Eng. Conf., 1, 193–207.

Goda Y., 2000, *Random seas and design of maritime structures*, World Sci. Publ., Singapore, 443 pp.

Grue J., Clamond D., Huseby M., Jensen A., 2003, *Kinematics of extreme waves in deep water*, Appl. Ocean Res., 25 (6), 355–366.

Grue J., Jensen A., 2006, *Experimental velocities and accelerations in very steep wave events in deep water*, Eur. J. Mech. B-Fluid., 25 (5), 554–564.

Gudmestad O. T., 1993, *Measured and predicted deep water wave kinematics in regular and irregular seas*, Mar. Struct., 6 (1), 1–73.

Hanson J. L., Phillips O. M., 1999, *Wind sea growth and dissipation in the open ocean*, J. Phys. Oceanogr., 29 (8), 1633–1648.

Hasselmann K., 1974, *On the spectral dissipation of ocean waves due to white capping*, Bound.-Lay. Meteorol., 6 (1–2), 107–127.

Hasselmann S., Hasselmann K., Allender J. H., Barnett T. P., 1985, *Computations and parameterizations of the non-linear energy transfer in a gravity wave spectrum. Part II: Parameterizations of the non-linear energy transfer for application in wave models*, J. Phys. Oceanogr., 15 (11), 1378–1391.

Holthuijsen L. H., 2007, *Waves in oceanic and coastal waters*, Cambridge Univ. Press, Cambridge, 387 pp.

Janssen P., 2004, *The interaction of ocean waves and wind*, Cambridge Univ. Press, Cambridge, 300 pp.

Jensen A., Clamond D., Huseby M., Grue J., 2007, *On local and convective acceleration in steep wave events*, Ocean Eng., 34 (3–4), 426–435.

Kharif C., Pelinovsky E., 2003, *Physical mechanisms of the rogue wave phenomenon*, Eur. J. Mech. B-Fluids, 22 (6), 603–634.

Kitaigorodskii S. A., 1983, *On the theory of the equilibrium range in the spectrum of wind-generated gravity waves*, J. Phys. Oceanogr., 13 (5), 816–827.

Komen G. J., Cavaleri L., Donelan M., Hasselmann K., Hasselmann S., Janssen P. A. E. M., 1994, *Dynamics and modelling of ocean waves*, Cambridge Univ. Press, Cambridge, 532 pp.

Komen G. J., Hasselmann S., Hasselmann K., 1984, *On the existence of a fully developed wind-sea spectrum*, J. Phys. Oceanogr., 14 (8), 1271–1285.

Kowalik Z., Knight W., Logan T., Whitmore P., 2005, *Numerical modeling of the global tsunami: Indonesian tsunami of 26 December 2004*, Sci. Tsunami Haz., 23 (1), 40–56.

Krasitskii V. P., 1994, *On reduced equations in the Hamiltonian theory of weakly non-linear surface waves*, J. Fluid Mech., 272, 1–20.

Krylov J. M. (ed.), 1986, *Wind, waves and marine ports*, Gidrometeoizdat, Leningrad, 264 pp., (in Russian).

Krylov J. M., Strekalov S. S., Tsyplukhin W. F., 1976, *Wind waves and their interaction with structures*, Gidrometeoizdat, Leningrad, 256 pp., (in Russian).

Kurkin A. A., Pelinovsky E. N., 2004, *Freak waves: Facts, theory and modelling*, Tech. Univ. Nizhny Novgorod, 157 pp., (in Russian).

Lake B. M., Yuen H. C., Rungaldier H., Ferguson W. E., 1977, *Nonlinear deep-water waves: Theory and experiment. Part 2. Evolution of a continuous wave train*, J. Fluid Mech., 83 (1), 49–74.

Lamb H., 1932, *Hydrodynamics*, Dover Publ., Inc., New York, 738 pp.

Lavrenov I. V., 2003, *Wind-waves in oceans. Dynamics and numerical simulation*, Springer-Verlag, Berlin, 376 pp.

LeBlond P. H., Mysak L. A., 1978, *Waves in the ocean*, Elsevier Oceanogr. Ser., 20, Elsevier, Amsterdam, 602 pp.

Lewis E. R., Schwartz S. E., 2004, *Sea salt aerosol production. Mechanisms, methods, measurements, and models*, Geophys. Monogr., Vol. 152, American Geophys. Union, Washington, 412 pp.

Lie V., Tørum A., 1991, *Ocean waves over shoals*, Coast. Eng., 15 (5–6), 545–562.

Lo F., Mei C. C., 1985, *A numerical study of water-wave modulation based on a high-order non-linear Schrödinger equation*, J. Fluid Mech., 150, 395–416.

Longuet-Higgins M. S., 1969, *On wave breaking and the equilibrium spectrum of wind-generated waves*, P. Roy. Soc. Lond. A Mat., 310 (1501), 151–159.

Longuet-Higgins M. S., 1978, *The instabilities of gravity waves of finite amplitude in deep water. II. Subharmonics*, P. Roy. Soc. Lond. A Mat., 360 (1703), 489–505.

Longuet-Higgins M. S., 1985, *Acceleration in steep gravity waves*, J. Phys. Oceanogr., 15 (11), 1570–1579.

Longuet-Higgins M. S., Cokelet E. D., 1976, *The deformation of steep surface waves on water. I. A numerical method of computation*, P. Roy. Soc. Lond. A Mat., 350 (1660), 1–26.

Longuet-Higgins M. S., Stewart R. W., 1964, *Radiation stress in water waves: A physical discussion with applications*, Deep-Sea Res., 11 (4), 529–562.

Luke J. C., 1967, *A variational principle for a fluid with a free surface*, J. Fluid Mech., 27 (2), 395–397.

Massel S. R., 1989, *Hydrodynamics of coastal zones*, Elsevier, Amsterdam, 316 pp.

Massel S. R., 1993, *Extended refraction-diffraction equations for surface waves*, Coastal Eng., 19 (1–2), 97–126.

Massel S. R., 1996, *Ocean surface waves: Their physics and prediction*, World Sci. Publ., Singapore, 491 pp.

Massel S. R., 2001, *Circulation of groundwater due to wave set-up on a permeable beach*, Oceanologia, 43 (3), 279–290.

Massel S. R., 2007, *Ocean waves breaking and marine aerosol fluxes*, Springer, New York, 323 pp.

Massel S. R., Gourlay M. R., 2000, *On the modelling of wave breaking and set-up on coral reefs*, Coast. Eng., 39 (1), 1–27.

Massel S. R., Pelinovsky E. N., 2001, *Run-up of dispersive and breaking waves on beaches*, Oceanologia, 43 (1), 61–97.

Massel S. R., Przyborska A., Przyborski M., 2004, *Attenuation of wave-induced groundwater pressure in shallow water. Part 1*, Oceanologia, 46 (3), 383–404.

Massel S. R., Przyborska A., Przyborski M., 2005, *Attenuation of wave-induced groundwater pressure in shallow water. Part 2. Theory*, Oceanologia, 47 (3), 291–323.

Mei C. C., 1989, *The applied dynamics of ocean surface waves*, World Sci. Publ., Singapore, 740 pp.

Mei C. C., Stiassnie M., Yue D. K.-P., 2006, *Theory and applications of ocean surface waves. Part 1: Linear aspects*, *Part 2: Nonlinear aspects*, Adv. Ser. Ocean Eng., Vol. 23, World Sci. Publ., Singapore, Vol. 1 – 1071 pp., Vol. 2 – 569 pp.

Miles J. W., 1957, *On the generation of surface waves by shear flows*, J. Fluid Mech., 3 (2), 185–204.

Monahan E. C., 1971, *Oceanic whitecaps*, J. Phys. Oceanogr., 1 (2), 139–144.

Monahan E. C., O'Muircheartaigh I., 1981, *Optimal power-law description of oceanic whitecap coverage dependence on wind speed*, J. Phys. Oceanogr., 10 (12), 2094–2099.

Moshagen H., Tørum A., 1975, *Wave induced pressure in permeable sea beds*, J. Waterway. Div. – ASCE, 101 (1), 49–57.

Ochi M. K., 1998, *Ocean waves. The stochastic approach*, Cambridge Univ. Press, Cambridge, 319 pp.

Ochi M. K., Tsai C.-H., 1983, *Prediction of occurrence of breaking waves in deep water*, J. Phys. Oceanogr., 13 (11), 2008–2019.

Onorato M., Osborne A. R., Serio M., Bertone S., 2001, *Freak waves in random oceanic sea states*, Phys. Rev. Lett., 86 (25), 5831–5834.

Onorato M., Osborne A. R., Serio M., Cavaleri L., Braudini C., Stansberg C. T., 2006, *Extreme waves, modulational instability and second order theory: Wave flume experiments on irregular waves*, Eur. J. Mech. B-Fluids, 25 (5), 586–601.

Onorato M., Osborne A. R., Serio M., Damiani T., 2000, *Occurrence of freak waves from envelope equations in random ocean wave simulations*, [in:] *Rogue waves 2000*, M. Olagnon & G. A. Athanassoulis (eds.), Edn. Ifremer, Brest, 181–192.

Pelinovsky E. N., 1996, *Tsunami waves hydrodynamics*, Inst. Appl. Phys., Nizhny Novgorod, 274 pp., (in Russian).

Phillips O. M., 1957, *On the generation of waves by turbulent wind*, J. Fluid Mech., 2 (5), 417–445.

Phillips O. M., 1977, *The dynamics of the upper ocean*, Cambridge Univ. Press, Cambridge, 336 pp.

Phillips O. M., 1985, *Spectral and statistical properties of the equilibrium range in wind-generated gravity waves*, J. Fluid Mech., 156, 505–531.

Rapp R. J., Melville W. K., 1990, *Laboratory measurements of deep-water breaking waves*, Philos. T. Roy. Soc. A, 331 (1622), 735–800.

Sarpkaya T., Isaacson M. St. Q., 1981, *Mechanics of waves forces on offshore structures*, Van Nostrand Reinhold, New York, 651 pp.

Smith S. F., Swan C., 2002, *Extreme two-dimensional water waves: An assessment of potential design solutions*, Ocean Eng., 29 (4), 387–416.

Snyder R. L., Smith L., Kennedy R. M., 1983, *On the formation of whitecaps by a threshold mechanism. Part III: Field experiment and comparison with theory*, J. Phys. Oceanogr., 13 (8), 1505–1518.

Sobey R. J., 1992, *A local Fourier approximation method for irregular wave kinematics*, Appl. Ocean Res., 14 (2), 93–105.

Song J.-B., Banner M. L., 2002, *On determining the onset and strength of breaking for deep water waves. Part I: Unforced irrotational wave groups*, J. Phys. Oceanogr., 32 (9), 2541–2558.

Srokosz M. A., 1986, *On the probability of wave breaking in deep water*, J. Phys. Oceanogr., 16 (2), 382–385.

Stoker J. J., 1957, *Water waves, the mathematical theory with applications*, Interscience Publ., Inc., New York, 567 pp.

Stramska M., Petelski T., 2003, *Observations of oceanic whitecaps in the north polar waters of the Atlantic*, J. Geophys. Res., 108 (C3), 3086, doi:10.1029/2002JC001321.

Svendsen I. A., 1984, *Wave heights and set-up in a surf zone*, Coast. Eng., 8 (4), 303–329.

Thorpe S. A., 1993, *Energy loss by breaking waves*, J. Phys. Oceanogr., 23 (11), 2498–2502.

Toba Y., 1973, *Local balance in the air-sea boundary process. III. On the spectrum of wind waves*, J. Oceanogr. Soc. Jpn., 29 (5), 209–220.

Tørum A., 2007, *Wave induced pore pressure–air/gas content*, J. Waterw. Port C. Div., 133 (1), 83–86.

Tørum A., Gudmestad O. T. (eds.), 1990, *Water wave kinematics*, Kluwer Acad. Publ., Dordrecht, 771 pp.

Trulsen K., Dysthe K. B., 1996, *A modified non-linear Schrödinger equation for broader bandwidth gravity waves on deep water*, Wave Motion, 24 (3), 281–289.

Trulsen K., Dysthe K., 1997, *Freak waves – a three-dimensional wave simulation*, Proc. 21 Symp. Nav. Hydrodyn., Nat. Acad. Press, 550–560.

Tulin M. P., Waseda T., 1999, *Laboratory observations of wave group evolution including breaking effects*, J. Fluid Mech., 378, 197–232.

WAMDI group: Hasselmann S., Hasselmann K., Bauer E., Janssen P. A. E. M., Komen G. J., Bertotti L., Lionello P., Guilaune A., Cordone V. C., Greenwood M., Reistad L., Zambresky L., Ewing J. A., 1988, *The WAM model: A third generation ocean wave prediction model*, J. Phys. Oceanogr., 18 (12), 1775–1810.

Waseda T., Tulin M. P., 1999, *Experimental study of the stability of deep-water wave trains including wind effects*, J. Fluid Mech., 401, 55–84.

Węsławski J. M., Urban-Malinga B., Kotwicki L., Opaliński K., Szymelfenig M., 2000, *Sandy coastlines – are there conflicts between recreation and natural values?*, Oceanol. Stud., 29 (2), 5–18.

Wheeler J. D., 1970, *Method for calculating forces produced by irregular waves*, Proc. Offshore Technol. Conf., 1, 71–82.

Xu D., Liu X., Yu D., 2000, *Probability of wave breaking and whitecap coverage in a fetch-limited sea*, J. Geophys. Res., 105 (C6), 14 253–14 259.

Zakharov V. E., 1968, *Stability of periodic waves of finite amplitude on the surface of a deep fluid*, J. Appl. Mech. Tech. Phy., 9 (2), 190–194.